



Published in final edited form as:

Nat Biomed Eng. 2021 November ; 5(11): 1306–1319. doi:10.1038/s41551-021-00799-6.

Elimination of acquired resistance to PD-1 blockade via the concurrent depletion of tumour cells and immunosuppressive cells

Gang Xue¹, Ziyu Wang¹, Ningbo Zheng¹, Jing Fang¹, Chengqiong Mao², Xiaoyin Li³, Guangxu Jin², Xin Ming², Yong Lu^{1,*}

¹Comprehensive Cancer Center, Wake Forest Baptist Health, Winston-Salem, NC, USA, 27157; Department of Microbiology & Immunology, Wake Forest School of Medicine, Winston-Salem, NC, USA, 27101

²Comprehensive Cancer Center, Wake Forest Baptist Health, Winston-Salem, NC, USA, 27157; Department of Cancer Biology, Wake Forest School of Medicine, Winston-Salem, NC, USA, 27157

³Department of Mathematics and Statistics, St. Cloud State University, St Cloud, MN, USA, 56301

Abstract

Antigen release resulting from the death of tumour cells induced by chemotherapies and targeted therapies can augment the antitumor responses induced by immune checkpoint blockade (ICB). However, tumours responding to ICB therapies often become resistant to them. Here, we show that the specific targeting of tumour cells promotes the growth of tumour-cell variants that are resistant to ICB, and that the acquired resistance can be overcome via the concurrent depletion of tumour cells and of major types of immunosuppressive cells via a monoclonal antibody binding the enzyme CD73 (which we identified is highly expressed on tumour cells and on regulatory T cells, myeloid-derived suppressor cells and tumour-associated macrophages, yet not on cytolytic T lymphocytes, natural killer cells and dendritic cells). In mice with murine tumours, the systemic administration of anti-PD1 antibodies and anti-CD73 antibodies conjugated to a near-infrared dye subverted near-infrared-irradiated tumours from acquiring resistance to ICB and resulted in the eradication of advanced tumours. The elimination of immunosuppressive cells may overcome acquired resistance to ICB across a range of tumour types and combination therapies.

The reinvigoration of tumor-specific T cells by immune checkpoint blockade (ICB) has recently demonstrated remarkable clinical efficacy across tumor types^{1,2}. Unfortunately, the

Users may view, print, copy, and download text and data-mine the content in such documents, for the purposes of academic research, subject always to the full Conditions of use: <https://www.springernature.com/gp/open-research/policies/accepted-manuscript-terms> **Reprints and permissions information** is available at www.nature.com/reprints.

*Corresponding authors, yolu@wakehealth.edu, **Correspondence and requests for materials** should be addressed to Y.L.

Author contributions

G.X. and Y.L. designed the experiments, analyzed the data, and wrote the paper. G.X. performed most of the experiments. G.J. helped with CyTOF data analysis. X.L. performed statistical analysis. J.F., Z.W., and N.Z. helped with animal studies. C.M. and X.M. provided technical support.

Competing interests

The authors declare no competing interests.

majority of patients do not respond to ICB and only a small percentage of them achieve durable benefits. For example, PD-1 blockade showed an overall response rate (ORR) of only 4.7% (complete response, CR: 1/170; partial response, PR: 7/170) in 170 patients with metastatic triple-negative breast cancer (TNBC)³, whereas PD-L1 and CTLA-4 blockade appears minimally active⁴. Similarly, to date, no response (0%) has been observed in clinical trials among patients with pancreatic ductal adenocarcinoma (PDAC) using anti-PD1⁵, anti-PD-L1⁶⁻⁷, or anti-CTLA-4⁸ ICB. Furthermore, with higher activity and broader use of ICB immunotherapies, the denominator of patients with a tumor response has increased and the chances of finding patients who responded for a period of time and then progressed, termed acquired resistance, increases⁹. One explanation for the low response rate is that the effects of ICB are negated by the presence of other immune tolerance mechanisms that keep the immune system in check in the tumor microenvironment (TME)¹⁰. Growing evidence suggests that tumor-infiltrating myeloid-derived suppressor cells (MDSCs), tumor-associated macrophages (TAM), and regulatory T cells (Tregs) cells contribute to immune tolerance and reduced CD8⁺ cytolytic T lymphocyte (CTL) induction, infiltration, and cytolytic function. Further, this immunosuppressive phenotype is not abolished by ICB when tumors fail to respond or acquire resistance to ICB therapy¹¹⁻¹⁶. However, the contribution of immunosuppressive cells in TME to acquired resistance of ICB immunotherapy is still elusive.

Abnormal differentiation and function of myeloid cells is a hallmark of cancer, which blocks CTL function and protects tumors from chemotherapy and immunotherapy¹⁷. Some strategies have been developed to prevent the accumulation of myeloid cells, or alternatively, inhibit myeloid cells' immunosuppressive activity¹⁸. Because myeloid cells are a heterogeneous population, approaches to specifically target MDSCs and TAMs without affecting other myeloid cells (such as dendritic cells (DCs)), or subverting CTL responses, remain to be developed and are critical to surmount ICB resistance. In addition to myeloid cells, the function of tumor-infiltrating CTLs may be also suppressed by nearby Tregs¹⁹. Controlling tumor-infiltrating Treg cells has been considered another essential step for successful immunotherapy²⁰. Since most Treg cell markers are presented on activated type 1 helper (Th1) and CTLs (e.g. CD25)²⁰, approaches are needed to selectively deplete or inhibit tumor-infiltrating Treg cells without dampening CTLs – but these approaches remain elusive. Because systematic depletion of immunosuppressive cells may result in severe autoimmunity²¹, ablation of all major types of immunosuppressive cells (e.g. MDSC, TAM, and Treg cells) in tumor may subvert resistance to ICB and bolster an unprecedented immunotherapeutic efficacy, which represents an unmet need for immunotherapy to modify the tumor immune landscape to overcome resistance mechanisms. Currently, approaches that specifically target a single type of immunosuppressive cell in TME remain to be achieved.

In this study, we demonstrated that targeting tumor cell-expressed antigen (e.g. B7H3) selected the outgrowth of resistant variant tumor cells and promoted resistant variant tumor outgrowth, despite co-administration of ICB. To address this acquired resistance, we identified CD73 as a common marker that is highly expressed by most types of immunosuppressive cells [e.g. Tregs, M2-like tumor-associated macrophages (TAM.M2), and myeloid-derived suppressor cells (MDSCs)] as well as by tumor cells, but not or very limited by anti-tumor immune cells, e.g. effector CD4⁺ T cells or CD8⁺ T cells. We thus

hypothesized that the killing of CD73⁺ cells in tumor may simultaneously deplete tumor cells and major types of immunosuppressive cells in TME, which may subsequently break the immune tolerance in tumor and overcomes the acquired resistance to ICB. To achieve this goal, we take advantage of an existing approach for near-infrared (NIR) activated photo-depletion of the target cells²²⁻²⁴ and create a IR-700 dye-conjugated anti-CD73 monoclonal antibody (α CD73-Dye). α CD73-Dye conjugates are able to specifically bind to CD73⁺ cells, and induces highly selective, necrotic cell death of CD73⁺ cells, without damaging adjoining cells after near-infrared (NIR 690 nm) exposure. When administered intravenously *in vivo*, local NIR exposure eradicated advanced murine tumors (EMT6, 4T1.2, MMTV-PyMT spontaneous TNBCs, and Pan02 PDAC) and together with α PD-1 monoclonal antibody (mAb) treatment, was associated with ~3 months of tumor-free survival in mice with both local tumors (NIR exposure) and remote tumors (no NIR exposure; serving as metastatic tumors). Furthermore, eradication of CD73⁺ cells also sensitized human PDAC patient-derived organotypic tumor spheroids to α PD-1 mAb therapy. Therefore, this study revealed a mechanism underlying acquired resistance of ICB immunotherapy and suggested a strategy for overcoming acquired resistance by locally removing all major types of immunosuppressive cells.

Results

Relapse of resistant tumors is inevitable when merely targeting a tumor-expressed antigen.

To understand the mechanism of acquired resistance in ICB, we utilized Pan02^{B7H3} cells-bearing mice (overexpression of B7H3 on Pan02 PDAC cells, Fig. 1a and Supplementary Fig. 1a). To achieve the goal of tumor-killing of Pan02^{B7H3} cells, we adopted an existing approach of NIR-activated photo-depletion of the target cells by using antibody-IR700 conjugates²³. α B7H3-Dye+NIR induced rapid cell necrosis in >98% of Pan02^{B7H3} tumor cells *in vitro* (Fig. 1b, c). Next, we inoculated Pan02^{B7H3} cells s.c. on the flank of mice. We found that the expression level of B7H3 on tumor-infiltrating immune cells was negative or very low (Supplementary Fig. 1b). Consistent with the low B7H3 expression level, α B7H3-Dye+NIR could not induce cell necrosis in these immune cells *ex vivo* (Supplementary Fig. 1c). When Pan02^{B7H3} cells were inoculated in mice, α PD-1 and α B7H3-Dye+ α PD-1 treatments did not show any measurable antitumor activity. Moreover, treatments with α B7H3-Dye+NIR or α B7H3-Dye+NIR+ α PD-1 induced an initial rapid regression of NIR-treated tumors; but all respondent tumors finally recurred in all treated mice and led to the death of all mice (Fig. 1d, e). The recurred progress was similar to the scenario of acquired resistance in the clinical setting, with a median survival time of 46.5 days for α B7H3-Dye+NIR and 48.5 days for α B7H3-Dye+NIR+ α PD-1 treated mice (Fig. 1d, e). We also used this approach to target B7H3-overexpressed EMT6^{B7H3} murine triple-negative breast cancer (overexpression of B7H3 on EMT6 TNBC cells, Fig. 1f and Supplementary Fig. 1a) and α B7H3-Dye+NIR induced rapid cell necrosis in >95% of EMT6^{B7H3} tumor cells *in vitro* (Fig. 1g). In this tumor model, α PD-1, α B7H3-Dye+ α PD-1, and α B7H3-Dye+NIR treatments induced a partial response initially in EMT6^{B7H3} tumor-bearing mice, but unfortunately, the development of acquired resistance eventually led to the tumor recurrence (Fig. 1h). Although α B7H3-Dye+NIR+ α PD-1 treatment could further

inhibit the growth of EMT6^{B7H3} tumors compared to α PD-1, α B7H3-Dye+ α PD-1, and α B7H3-Dye+NIR treatments, but all respondent tumors finally recurred (Fig. 1h).

We next inoculated two Pan02^{B7H3} tumors s.c. on the left and right flanks of mice, and performed the α B7H3-Dye+NIR+ α PD-1 treatment (irradiation on the left-side tumor only; right-side tumors were shielded from light). We then tested the sensitivity of local NIR exposed (Left) tumors and the remote no NIR-treated (Right) tumors when the left tumor relapsed (on day 19) by retreatment with α B7H3-Dye+NIR irradiation (Fig. 1i). Local recurrent tumors (Left) but not remote tumors (Right) were resistant (Fig. 1j, k). We thus hypothesize that local recurrent tumors would be B7H3-loss variant tumors iteratively selected by α B7H3-Dye+NIR targeting B7H3, as often occurs in clinical cancer targeted therapy. To test our hypothesis, we harvested PBS-treated Pan02^{B7H3} tumor, Pan02 tumor, locally recurrent Pan02^{B7H3} tumor, and remote Pan02^{B7H3} tumor tissues on day 19. qPCR demonstrated that only locally relapsed Pan02^{B7H3} tumors showed largely downregulated *B7h3* levels (Supplementary Fig. 1d). Similarly, recurred EMT6^{B7H3} tumors after α B7H3-Dye+NIR+ α PD-1 treatment also display substantially reduced *B7h3* levels (Supplementary Fig. 1e). Taken together, these results demonstrate that targeting cancer cells would select and promote the outgrowth of resistant variant tumor cells and it seems that the formation of acquired resistant tumors is inevitable, even though ICB was co-administered.

Identification of common marker(s) to target major types of immunosuppressive cells.

Because tumor contains a large number of infiltrated immunosuppressive cells which may dampen the efficacy of immunotherapy²⁵, we hypothesize that additional targeting of immunosuppressive cells in TME would overcome the acquired resistance to ICB. To identify a common marker highly expressed on major types of immunosuppressive cells to specifically target immunosuppressive cells, we analyzed gene expression of Treg cells, MDSCs, and TAM.M2 cells compared to Th1 cells, DCs, and normal tissue macrophages, respectively, based on the published microarray data^{26–28}. Clustering analysis indicated that Treg cells, MDSCs, and TAM.M2 cells have very different gene signatures compared to Th1 cells, DCs, and tissue macrophages, respectively (Fig. 2a, b, c). Overlap among upregulated genes (>2-fold upregulation) in Treg cells/Th1, MDSCs/DCs, and TAM.M2/tissue macrophages were further analyzed by Venn diagram. We identified 11 genes that were co-expressed in these immunosuppressive cells compared to non-immunosuppressive cells (Fig. 2d). The 11 genes were further ranked by integrating their fold-changes in the comparisons of “immunosuppressive to non-immunosuppressive cells” and the overall gene expression level change was evaluated by a rank-adjusted fold-change (see methods section for details). This analysis identified *Nt5e* gene (encodes CD73 protein) as the top candidate far exceeding 10 other genes (Fig. 2e); this finding is also in agreement with previous studies^{29,30}. We next verified the expression of CD73 on the different types of immune cells in EMT6 TME by FACS, and confirmed that surface CD73 expression was high in multiple types of immunosuppressive cells (e.g. Treg cells, MDSCs, and TAM.M2 cells, Fig. 2f and Supplementary Fig. 2a), while such expression was negative or very low for DCs or effector immune cells (e.g. effector CD4⁺ T cells, CD8⁺ T cells, or NK cells) (Supplementary Fig. 2b). Thus, CD73 may provide us with an opportunity to selectively deplete all major types of immunosuppressive cells in TME to modify the tumor immune landscape.

Because multiple types of cancer cells have been reported to express surface CD73^{31,32}, we thus analyzed the expression of CD73 by murine cancer cell lines. Interestingly, CD73 is highly expressed on the surface of all murine 4T1.2 TNBC cells, ~75% of murine EMT6 TNBC cells, while such expression is negative for murine Pan02 PDAC cells (Fig. 2g and Supplementary Fig. 2c). To achieve the goal of local tumor killing of CD73⁺ cells, we created α CD73-Dye conjugates and performed α CD73-Dye-mediated NIR irradiation. α CD73-Dye+NIR induced rapid cell necrosis in >99% of 4T1.2 tumor cells (CD73⁺) and ~75% of EMT6 tumor cells but did not induce cell death of Pan02 tumor cells (CD73⁻) (Fig. 2h, i and Supplementary Fig. 2d). These results suggest that the rapid killing of tumor cells after NIR exposure depends on CD73 expression. We next explored the effects of α CD73-Dye+NIR on EMT6 tumor-isolated immune cells *in vitro*. In correlation with their surface expression of CD73, α CD73-Dye+NIR also rapidly killed immunosuppressive cells, including Treg cells, MDSCs, and TAM.M2, (Fig. 2i and Supplementary Fig. 2e), while leaving intact CTLs (effector CD4⁺ T cells and CD8⁺ T cells), NK cells or DCs (Supplementary Fig. 2e). These data suggest that CD73-Dye can eliminate tumor cells and the major types of immunosuppressive cells in the TME simultaneously, in a highly specific manner.

Based on the efficient killing capacity of α CD73-Dye+NIR *in vitro*, we performed a study in a 4T1.2 orthotopic TNBC model to test the antitumor function of α CD73-Dye+NIR *in vivo*. We firstly chose 4T1.2 as they express high amounts of CD73 on the cell surface. BALB/c mice bearing advanced 4T1.2 tumors (~7×6 mm) in mammary pad were i.v. injected with α CD73-Dye, and on the next day, tumors were exposed to 690nm NIR-light. All other parts of mice were covered with an aluminum film to avoid light exposure (Extended Data Fig. 1a). Treatments were performed once again for a group of mice four days later. Remarkably, NIR with α CD73-Dye exposure eradicated the advanced tumors, while IgG-Dye+NIR or α CD73-Dye (no NIR) did not display measurable antitumor activity (Extended Data Fig. 1b). In addition, we also explored the potential of α CD73-Dye on tumors formed by injection of Pan02 cells, which do not produce CD73. The Pan02 PDAC tumor model employs a transplantable form of murine PDAC refractory to many standard chemotherapeutic agents and ICB^{33,34}. Pan02 tumor-bearing C57BL/6 mice were given one or two doses of α CD73-Dye-mediated NIR irradiation when tumors reached ~7×6 mm. Surprisingly, α CD73-Dye-mediated NIR irradiation also largely reduced the tumor growth of Pan02 tumors (Extended Data Fig. 1c); a result that may be arising from intratumor depletion of CD73⁺ immunosuppressive cells. Taken together, our results indicate that α CD73-Dye efficiently killed CD73⁺ immunosuppressive cells and cancer cells, and mediated extraordinary therapeutic effects to tumors established from both CD73⁺ and CD73⁻ tumor cells.

Targeting CD73⁺ cells modifies the tumor immune landscape and bolsters CTL responses *in vivo*.

The robust antitumor function on tumors prompted us to analyze the 4T1.2 TME after α CD73-Dye-mediated NIR irradiation. We first performed mass cytometry (CyTOF) to profile the tumor immune cell lineages, and the results revealed some remarkably features associated with antitumor immunity activation. α CD73-Dye-mediated NIR irradiation

preferentially reduced multiple types of immunosuppressive cells in tumors, including ~85% reduction of Treg cells, 80% reduction of TAM.M2, and 95% reduction of MDSCs. Notably, the reduction of immunosuppressive cells was accompanied by a marked increase in tumor-infiltrating CD8⁺ CTLs, nearly a 50-fold increase compared to other treated groups (Fig. 3a, b). We further calculated the ratio of CD8⁺ T cells to different types of immunosuppressive cells. Depletion of CD73⁺ cells resulted in ~6 to 200-fold increase in the CD8⁺/Treg cells, CD8⁺/TAM.M2, CD8⁺/PMN.MDSC and CD8⁺/MoMDSC ratios over control groups (Extended Data Fig. 2a, b, c, d). Similar to CD8⁺ T cells, the modifications of tumor immune landscape also largely increase the ratio of NK cells or CD4⁺ effector T cells to various types of immunosuppressive cells (Extended Data Fig. 2e, f, g, h, i). Finally, the clearance of immunosuppressive cells may create a highly activating tumor milieu to allow for tumor-infiltrating CD8⁺ CTL reinvigoration; and indeed, remarkably upregulated GzmB- and IFN- γ -producing CTLs were detected after α CD73-Dye+NIR irradiation (Extended Data Fig. 2j, k). In addition to 4T1.2 tumors, we also analyzed the immune landscape after α CD73-Dye-mediated NIR irradiation in EMT6 TME. Similar to 4T1.2 tumor model, we found that α CD73-Dye-mediated NIR irradiation preferentially reduced multiple types of immunosuppressive cells in tumors but induced a marked increase in tumor-infiltrating CD8⁺ CTLs (Fig. 3c–3d). Overall, our data thus far highlight that depletion of CD73⁺ cells by α CD73-Dye+NIR in TME drives CTL reinvigoration for immune elimination of tumor cells.

α CD73-Dye plus local NIR irradiation favors systemic CTL responses.

Because NIR irradiation may not reach metastatic tumors, we sought to determine whether local α CD73-Dye+NIR irradiation facilitates systemic CTL activation, which may be crucial for metastatic tumor clearance. Therefore, we performed a series of experiments to evaluate the potential CTL activation and tumor-infiltration in tumors with and without direct α CD73-Dye+NIR irradiation. We inoculated two Pan02^{OVA} tumors s.c. on the left and right flanks of mice, and performed the α CD73-Dye+NIR irradiation on the left-side tumor only (right-side tumors were shielded from light). One day after NIR irradiation, we adoptively transferred luciferase-transduced OVA-reactive OT-I T cells via tail vein, which provides an approach to visualize the tumor-specific CD8⁺ CTL trafficking and accumulation (Fig. 4a). To our surprise, bioluminescent imaging revealed that massive Luc⁺ OT-I T cells infiltrated not only in the α CD73-Dye irradiated tumor but also the tumor shielded from light (Fig. 4b, c). Consistently, there are substantially more OT-I T cells after α CD73-Dye+NIR treatment as calculated for the absolute number of these tumor-specific T cells by FACS (Fig. 4d).

To further confirm the induction of tumor-specific CD8⁺ CTL response by α CD73-Dye+NIR irradiation *in vivo*, we labeled OT-I CD8⁺ T cells with CFSE and adoptively transferred them to mice bearing two Pan02^{OVA} tumors one day after the irradiation on the left tumor (No NIR exposure on the right tumor). Three days after the OT-I T cell transfer, α CD73-Dye+NIR irradiation stimulated a strong proliferation of OT-I T cells in tumor-draining lymph nodes (TDLNs) of tumors with and without the direct NIR exposure (Fig. 4e, f). Moreover, in mice bearing orthotopic and lung metastatic EMT6 and 4T1.2 TNBC, α CD73-Dye+NIR irradiation on the orthotopic tumor also greatly induced a robust effector CD8⁺ T cells response in the EMT6 lung metastatic tumor tissues (Fig. 4g) and

boosted the 4T1.2-specific CTL infiltrating in the 4T1.2 lung metastatic tumor tissues as measured by the gp70-tetramer⁺ CD8⁺ T cells (gp70 is a native antigen expressed by 4T1.2) (Fig. 4h), respectively. Critically, these studies identify the unique capacity of α CD73-Dye+NIR irradiation in driving robust host antitumor CTL responses.

α CD73-Dye+NIR irradiation overcomes the acquired resistance of ICB immunotherapy.

We first tested the anti-tumor efficacy of α CD73 and α CD73+ α PD-1 using 4T1.2 orthotopic TNBC model, because these therapies alone may repress tumor growth^{35,36}. In line with others^{35,36}, α CD73 or α CD73+ α PD-1 treatment exerted moderated but notable antitumor effects if treatments were started when 4T1.2 tumor size reached $\sim 3 \times 3$ mm (small early-stage tumors). However, neither α CD73 nor α CD73+ α PD-1 treatment display apparent antitumor function once treatment started when 4T1.2 tumors reached an advanced stage with a $\sim 7 \times 6$ mm tumor size (Supplementary Fig. 3). Although targeting CD73 enzyme activity is insufficient to control advanced tumors, we here repurposed anti-CD73 mAbs to deplete CD73⁺ cells by α CD73-Dye+NIR in tumor to determine if this strategy could overcome the acquired resistance. In mice bearing advanced orthotopic and lung metastatic EMT6 tumors (Fig. 5a), α PD-1, α CD73-Dye+ α PD-1, and α CD73-Dye+NIR treatments could induce initial tumor regression in EMT6 tumor-bearing mice, with the median survival time for 30.5, 30, and 47 days, respectively (22 days for IgG group). Remarkably, combo therapy (α CD73-Dye+NIR+ α PD-1, the same after) eradicated both advanced orthotopic EMT6 tumor (with NIR) and lung metastatic tumors (no direct NIR to lung) (Fig. 5b, c) and resulted in tumor-free survival of at least 90% of mice up to 100 days (Fig. 5d). Similar results were obtained in 4T1.2 tumor-bearing mice (Extended Data Fig. 3), further highlighting that α CD73-Dye+NIR subverts systemic α PD-1 ICB primary and acquired resistances and promotes curative responses. Although injection of α CTLA-4, α TIM-3, α TIGIT, α LAG3, α GITR, α OX40, or α 4-1BB also improves the antitumor effects of α CD73-Dye+NIR, none of these combinations resulted in the curative response as seen in α CD73-Dye+NIR+ α PD-1 combo therapy. In addition to TNBC models, we also tested the murine Pan02^{B7H3} and Pan02 tumors, which displayed resistance to IgG, α PD-1, and α CD73-Dye+ α PD-1 treatments (31, 32.5, 34 median survival time, respectively), but responded to α CD73-Dye+NIR treatment with ~ 50 days median survival time (Fig. 5e, h and Extended Data Fig. 4a, b, c, d). Similarly, α CD73-Dye+NIR+ α PD-1 combo therapy also produced a curative effect on established Pan02^{B7H3} tumors and Pan02 tumors at both the NIR exposed and the distant no NIR-treated sites and resulted in tumor-free survival of all treated mice (Fig. 5e, h and Extended Data Fig. 4a, b, c, d). Finally, host CTL responses dictate these extraordinary antitumor functions, because depletion of CD8⁺ T cells but not depletion of CD4⁺ T cells or NK cells dampens the curative responses (Extended Data Fig. 4e, f).

Depletion of immunosuppressive cells is indispensable for overcoming acquired resistance.

To dissect depletion of which cell type(s) is crucial to the observed curative responses, we used EMT6-bearing *Nt5e*^{-/-} BALB/c mice (host CD73 KO) to receive α CD73-Dye+NIR+ α PD-1 combo treatment, in which the immunosuppressive cells do not express CD73, a similar scenario of only targeting of tumor cells without depletion of

immunosuppressive cells. Consistently, α CD73-Dye+NIR+ α PD-1 combo treatment induced a notable tumor regression by killing CD73 expressing EMT6 cells, however, host deficiency of CD73 nullified the curative response (Fig. 6a, b). These results demonstrate that only targeting tumor cells without killing immunosuppressive cells invariably leads to acquired resistance. Conversely, we also used EMT6 CD73 knockout (EMT6^{CD73 KO}) tumor cells to establish tumors in WT BALB/c mice, in which tumor cells can not be directly eliminated by α CD73-Dye+NIR *in vitro* (Extended Data Fig. 5a, b). Interestingly, α CD73-Dye+NIR+ α PD-1 combo treatment also eradicated EMT6^{CD73 KO} tumors in WT mice for tumor-free survival in 85% of mice at day 50 (Extended Data Fig. 5c), suggesting that tumor cell-expression of CD73 may be only required for the optimal antitumor capacity of α CD73-Dye+NIR+ α PD-1 combo therapy.

To further elucidate whether removing all immunosuppressive cells, such as TAM.M2, Tregs, and MDSCs, is required for curative responses, we sorted immunosuppressive cells (Tregs, TAM.M2, or MDSCs) from orthotopic EMT6 tumors inoculated on WT or *Nt5e*^{-/-} BALB/c mice. We intratumorally injected one type of these sorted immunosuppressive cells into orthotopic EMT6 tumors inoculated in WT BALB/c mice one day before α CD73-Dye+NIR+ α PD-1 combo treatment, which establishes the scenario of only one type of immunosuppressive cell remaining as a result of the killing of all the other cell types. The numbers of intratumorally injected cells were adjusted to result in an equal/similar tumor “infiltration” of each subset of cells in WT *vs* *Nt5e*^{-/-} cell portion. Interestingly, injection of any type of *Nt5e*^{-/-} immunosuppressive cells, including Tregs, TAM.M2, or MDSCs, abrogated the curative capacity of the α CD73-Dye+NIR+ α PD-1 combo therapy (Fig. 6c), suggesting that targeting all types of these immunosuppressive cells is indispensable for subverting acquired resistance to ICB. Collectively, α CD73-Dye+NIR therapy subverts acquired resistance to ICB and bolsters an unexpectedly immunotherapeutic efficacy in EMT6 tumor model.

α CD73-Dye+NIR irradiation synergizes with α PD-1 to eradicate spontaneous tumors and human organotypic tumor spheroids.

Last, we assessed the anti-tumor capacity of α CD73-Dye+NIR+ α PD-1 combo therapy in a more difficult scenario of spontaneous TNBC tumor model (MMTV/PyVT) that is known to resistant to α PD-1 ICB³⁷. MMTV/PyVT mice, which can develop highly invasive mammary ductal carcinomas with a high frequency of lung metastases, highly resembles human luminal breast cancer³⁸. All-female carriers develop palpable mammary tumors by 6 to 7 weeks of age and tumors eventually develop in all of their 10 mammary fat pads³⁹. The treatments were started when mice developed 2 to 3 tumors ~60mm³ each, and NIR irradiation was performed on all of these tumors. Remarkably, only α CD73-Dye+NIR+ α PD-1 combo therapy eradicated these established spontaneous tumors (Fig. 7a); and also retarded the growth of tumors from other mammary glands (Fig. 7b, c, d). Furthermore, the eradication of the orthotopic tumors also led to the elimination of lung metastatic TNBCs, and most importantly, α CD73-Dye+NIR+ α PD-1 combo therapy resulted in an 80% survival rate at day 110 (Fig. 7e, f). These results highlight that α CD73-Dye+NIR irradiation holds promise for overcoming systematic resistance to α PD-1 therapy in mice genetically prone to spontaneous breast cancer.

Based on the Human Protein Atlas (HPA) dataset⁴⁰, most human cancer tissues display strong to moderate membranous and cytoplasmic CD73 positivity (Extended Data Fig. 6a). We also tested the expression of CD73 and B7H3 on immune cells and cancer cells in human PDAC tumor specimens. We found that cancer cells express CD73 and B7H3 and all major types of immunosuppressive cells displayed a high expression of CD73, but a low or no expression of B7H3 (Extended Data Fig. 6b, c). We next extend our study to test the antitumor capacity of α CD73-Dye+NIR+ α PD-1 and α B7H3-Dye+NIR+ α PD-1 combo therapy in human PDAC. To better evaluate the potential of combo therapy in a model that closely resembles the clinical setting, we used human PDAC patient-derived organotypic tumor spheroids (OTS) (Extended Data Fig. 6d). In agreement with our murine tumor model results, only α CD73-Dye+NIR+ α PD-1 combo therapy displayed robust tumor-killing ability in human PDAC (Extended Data Fig. 6e), suggesting that the combo therapy may have high translational potential as a therapy for human cancer.

Discussion

In this study, we demonstrated that acquired resistance may occur during ICB immunotherapy or combinational target therapy with ICB immunotherapy, and revealed a potential role of immunosuppressive cells in TME that leads to recurrence. Our results also suggest a strategy for overcoming acquired resistance by local removing all major types of immunosuppressive cells. By identification of CD73 as a common marker highly expressed on multiple types of immunosuppressive cells by bioinformatics analysis, we repurposed anti-CD73 mAbs from blocking the enzymatic activity of CD73 into the killing of CD73⁺ tumor and immunosuppressive cells by α CD73-Dye+NIR to overcome systemic ICB primary and acquired resistance. Remarkably, depleting of all major types of immunosuppressive cells eradicated advanced tumors, overcame acquired resistance of ICB immunotherapy, and induced curative responses in TNBC and PDAC tumor models.

Acquired resistance may cause cancer treatment failure and death in over 90% of patients with advanced tumors. Patients may initially respond to treatment, but recurrence often occurs because of the heterogeneous nature of cancer cell populations⁴¹. In heterogeneous cancer cells, the few cells that are resistant due to somatic mutation will be iteratively selected and escape during treatment⁴¹. Tumor cell death induced by chemotherapy- or targeted therapy is thought to promote tumor antigen presentation, which then facilitates the antitumor response of ICB. Interestingly, our results demonstrated that targeting tumor cell-expressed antigens (e.g. target B7H3 by α B7H3-Dye+NIR+ α PD-1) without destroying the immunosuppressive TME promoted the outgrowth of B7H3⁻ resistant tumor cells, akin to acquired resistance in the clinical setting⁴²⁻⁴⁴.

Various types of tumor-infiltrating immunosuppressive cells, including Treg cells, MDSCs, and TAM.M2, contribute to reduced CTL induction, infiltration, and cytolytic function, which dampens the responsiveness to ICB¹¹⁻¹⁶. The precise understanding of immunosuppressive cells to acquired resistance of ICB immunotherapy remains elusive. We hypothesized that depleting all major types of immunosuppressive cells may overcome the acquired resistance in ICB immunotherapy. Currently, approaches that specifically target a single type of immunosuppressive cell in TME have not yet been achieved. Here, we

identified that CD73 was highly expressed by all major types of immunosuppressive cells by comparing gene profiles of immunosuppressive cells to effector immune cells. We also confirmed that immunosuppressive cells, such as MDSCs, Treg cells, and TAMs.M2 highly expressed CD73, whereas the expression of CD73 on CD8⁺ CTL, Foxp3⁻CD4⁺ T cells, or DCs are negative or very low. This unique character of immunosuppressive cells provides us with a chance to simultaneously targeting these immunosuppressive cell subsets, which may contribute to the acquired resistance of ICB.

Indeed, CD73 is the main extracellular source of adenosine, and the accumulated extracellular adenosine could impair the cytotoxic potential of CD8⁺ T cells and NK cells in TME⁴⁵. A recent study also suggested that high expression of CD73 in immunosuppressive cells in tumor, particularly in TAM.M2, contributed to the lack of T-cell infiltration, thereby leading to poor clinical outcomes^{29,30}. Thus, the anti-CD73 antibody has been used to target the enzyme activity of CD73 for cancer treatment⁴⁶⁻⁴⁸, but unfortunately, the response of advanced tumors to α PD-1+ α CD73 antibody or α PD-1+adenosine antagonist is limited in both pre-clinic studies and clinic trials (clinical effectiveness data don't support launching a phase III study)^{36,49,50}. However, in our current study, we alternatively targeted CD73⁺ cells with α CD73-Dye+NIR to induce complete response and prevent the recurrence in ICB immunotherapy. This antitumor effect is associated with rapid killing of CD73⁺ tumor cells and immunosuppressive cells (including Treg cells, MDSCs, and TAMs.M2 cells), but no or very limited cytotoxicity to effector CD4⁺ T cells and CD8⁺ T cells or DCs, which is correlated with the surface expression level of CD73. To our surprise, targeting all major types of these immunosuppressive cells, including Treg, MDSC, TAM.M2, is indispensable for subverting acquired resistance to ICB, because the presence of any single type of immunosuppressive cells, including Tregs, TAM.M2, or MDSCs, in local TME abrogated the curative response.

Another intriguing finding is that α CD73-Dye+NIR+ α PD-1 also eradicated advanced tumors established from CD73⁻ tumor cells. These results suggest the importance of eradicating immunosuppressive cells to overcome acquired resistance, further highlighting the antitumor potential of α CD73-Dye in a range of tumor types, irrespective of the expression levels of CD73 on tumor cells. Although α CD73-Dye may also kill CD73⁺ cancer-associated fibroblasts (CAF) and cancer-associated endothelial cells (CAE)^{51,52}, it seems that removal of these cells is insufficient to prevent tumor recurrence. This is because B7H3 is also highly expressed on CAF and CAE⁵³, whereas α B7H3-Dye+NIR+ α PD-1 failed to induce tumor-free responses.

Based on the Human Protein Atlas (HPA) dataset⁴⁰, most cancer tissues display moderate to strong cytoplasmic and membranous CD73 positivity, with only lymphomas and testicular cancers being weakly positive or having no expression. Based on HPA dataset⁴⁰, normal human pancreatic tissues do not express detectable RNA levels of *Nt5e* (CD73 encoding gene), and normal human skin and breast tissues produce very low/limited *NT5E*. Similar results can be found in other databases (Fantom and GTEx)^{54,55} that normal human pancreas, skin, and breast tissues express very low to undetectable RNA level of *Nt5e*. Although some studies reported that some cells, like endothelial cells and hepatocytes⁵⁶, express some level of CD73, and therefore incur unintended toxicity when receiving

α CD73-Dye+NIR, NIR light irradiation can be carried out through a fiber optic diffuser under endoscopic guidance to specific target tumor sites and reduce potential damage to normal cells. These data suggest that some tumor types, e.g. PDAC, skin cancer, head and neck cancer, and breast cancer, may be good targets for local α CD73-Dye+NIR irradiation to eliminate the tumor and immunosuppressive cells in TME with limited damage to normal cells. Furthermore, local photodynamic therapy has been performed in patients with PDAC, using laser fibers inserted through needles positioned percutaneously through the anterior abdominal wall guided by ultrasound and computed tomography⁵⁷. Finally, NIR irradiation with antibody-Dye conjugates is now being tested in phase II clinical trials (NCT02422979; anti-EGFR-IR700), indicating that our proposed approach is feasible.

Taken together, we revealed an immunosuppressive cell-mediated acquired resistance in ICB immunotherapy. Our study provides an opportunity to preferentially and simultaneously target cancer cells and the immunosuppressive TME by our α CD73-Dye, which is sufficient in overcoming acquired resistance and triggers a system curative response in α PD-1-resistant tumors. Thus, this translationally relevant work will lay the critical foundation for future clinical trials for TNBC, PDAC, and other cancers.

Methods

Mice.

C57BL/6, BALB/c, C57BL/6-Tg(TcraTcrb)1100Mjb/J, B6.129S1-*Nt5e*^{tm1Lft}/J, B6.SJL-*Ptprc*^a *Pepc*^b/BoyJ, FVB/N-Tg(MMTV-PyVT)634Mul/J were purchased from The Jackson Laboratory. *Nt5e*^{-/-} mice in BALB/c background were generated by crossing *Nt5e*^{-/-} B6 mice with BALB/c mice for 12 generations. Male and female 6- to 8-week-old mice were used for PDAC animal experiments, whereas only female mice were used for TNBC models. All experiments complied with protocols approved by the Institutional Animal Care and Use Committee and Institutional Review Board at the Wake Forest School of Medicine.

Cell lines.

4T1.2 cell line was a gift from Dr. Robin L Anderson, University of Melbourne. Pan02 cell line was a gift from Dr. Qing Yi, Cleveland Clinic. EMT6 cell line was purchased from ATCC. Pan02^{B7H3} and EMT6^{B7H3} cell lines were generated by transducing with lentivirus vectors encoding murine B7H3. EMT6^{CD73 KO} cells were generated using CRISPR/Cas9 for CD73 deletion. Cells were cultured in RPMI 1640 Medium (Invitrogen) supplemented with 10% heat-inactivated fetal bovine serum (Thermo Scientific), 100 U/ml penicillin-streptomycin, and 2 mM L-glutamine (both from Invitrogen).

Reagents.

ViaStain AO/PI Staining Solution (catalog#CS2-0106) was purchased from Nexcelom. Propidium Iodide Solution (catalog#421301) was purchased from BioLegend. CellTrace CFSE Cell Proliferation Kit (catalog#C34554) was purchased from ThermoFisher. LIVE/DEAD Fixable Blue Dead Cell Stain Kit (catalog#L23105) was purchased from ThermoFisher. Anti-mouse CD73 antibody (clone: TY/23, catalog#BE0209), Anti-mouse B7H3 antibody (clone: MJ18, catalog#BE0124), anti-mouse PD-1 antibody

(clone: RMP1-14, catalog#BE0146), anti-mouse CTLA-4 antibody (clone: UC10-4F10-11, catalog#BE0032), anti-mouse TIM-3 antibody (clone: RMT3-23, catalog#BE0115), anti-mouse TIGIT antibody (clone: 1G9, catalog#BE0274), anti-mouse LAG-3 antibody (clone: C9B7W, catalog#BE0174), anti-mouse GITR antibody (clone: DTA-1, catalog#BE0063), anti-mouse OX-40 antibody (clone: OX-86, catalog#BE0031), anti-mouse 401BB antibody (clone: LOB12.3, catalog#BE0169), anti-mouse NK1.1 antibody (clone: PK136, catalog#BE0036), anti-mouse CD4 antibody (clone: GK1.5, catalog#BE0003-1), and anti-mouse CD8 antibody (clone: 2.43, catalog#BE0061) were purchased from BioXcell. Anti-human PD-1 (Nivolumab, catalog#A2002) was purchased from Selleckchem. Anti-human CD73 (clone: AD2, catalog#344002) was purchased from BioLegend.

Quantitative PCR.

Total RNA was extracted from the tumor using the TRIzol Reagent (Thermo Fisher), followed by cDNA synthesis with the High-Capacity cDNA Reverse Transcription kit (Applied Biosystems). qPCR was conducted with SYBR Select Master Mix (Applied Biosystems). Expression was normalized to the expression of the housekeeping gene β -actin. *mB7H3* forward: 5'-ATGCTTCGAGGATGGGGTG-3', *mB7H3* reverse: 5'-CCAGGCTCTGGGGAAAAGG-3'; *m β -actin* forward: 5'-GGCTGTATTCCCCTCCATCG-3', *m β -actin* reverse: 5'-CCAGTTGGTAACAATGCCATGT-3'.

Venn diagram analysis based on Cut-tree algorithm.

To compare the gene expression profiles of Treg cells, MDSCs, and TAM.M2 cells to Th1 cells, DCs, and normal tissue macrophages, we utilized un-supervised hierarchical clustering to all genes (>2 fold increase) in the published microarray data. The upregulated genes (>2 fold increase) in Treg cells, MDSCs, and TAM.M2 cells were taken for commonality analysis by Venn graph. Venn diagram analysis was implemented by VennDiagram in R (<https://www.r-project.org/>) as described before⁵⁸.

Rank-adjusted fold-change analysis.

Genes were sorted by the extent of the genes that show strong gene expression changes in the 3 comparisons of “non-immunosuppressive to immunosuppressive cells”. We defined the rank by sorting n_i from high to low:

$$n_i = \sum_{j=1}^3 S_{ij}$$

where $S_{ij} = \begin{cases} 0 & \text{if } FC_{ij} < 5 \\ 1 & \text{else} \end{cases}$, i is the gene i , and the FC_{ij} is the gene expression fold-change of i in the comparison of j .

The rank-adjusted fold-change (or called overall fold-change) integrated from the 3 comparisons is defined as follows,

$$FC_i = n_i \cdot \left(\frac{\sum_{j=1}^3 S_{ij} \cdot F_{ij}}{3} \right)$$

Flow cytometry.

Tumors were dissected, manually dissociated, and digested enzymatically with Collagenase D (Sigma) and DNase I (Roche) in PBS containing 2% FBS for 20 min at room temperature. EDTA was added to a final concentration of 10mM and incubate at room temperature for an additional 5 minutes. The entire suspension was filtered through a 70- μ m cell strainer to obtain a single-cell suspension. FITC-, PE- APC-, or eFluor-conjugated mAbs (1:100 dilution) were used for staining after Fc blocking. Samples were acquired with Fortessa flow cytometer or sorting, data were analyzed with Flowjo software. For T cell proliferation assay, 1 million OT-I T cells were labeled with 1.5 mM carboxyfluorescein diacetate succinimidyl ester (CFSE; Invitrogen), and then were adoptively transferred into tumor-bearing mice after NIR treatment. T cell proliferation in tumor-draining lymph nodes was determined 3 days after T cell transfer and ~4,500 OT-I T cells were analyzed (if less than 4,500 OT-I cells, all cells in the sample were collected and analyzed by FACS). The proliferation index is calculated as the average number of divisions of CFSE stained T cells in TDLNs⁵⁹.

Synthesis of IR700-Dye conjugated antibodies.

IR700-Dye conjugated antibodies were prepared using IRDye® 700DX Protein Labeling Kits (catalog#928-38046, Licor). In brief, antibodies were incubated with IRDye® 700DX NHS Ester at room temperature in phosphate buffer (pH 8.0) for 1h. The product of the conjugation was then purified with Zeba™ Spin Desalting Column. The antibody concentrations were determined with BCA protein assay kit (catalog#23225, Thermo Fisher), and the concentration of IR700 was determined by measuring the absorption at 689nm. The number of IR700 molecules conjugated to each antibody was calculated as reported by us and others^{24,60}. Antibody conjugates used in this study contain an average of 3.5 molecules of IR700 on each antibody.

Cell live/dead assay.

Cancer cells or sorted immune cells (1×10^4) were plated into 96 well plates and incubated with IgG, IgG-Dye, α B7H3-Dye, or α CD73-Dye at 5 μ g/mL for 6 hours at 37°C with 5% CO₂. The cells were then washed with cold PBS twice and cultured with phenol red-free culture medium. Cells were then irradiated with a NIR light-emitting diode at wavelengths of 690nm (catalog#L690-66-60; Marubeni America Co.). To measure the cytotoxic effect of NIR, cells were stained with PI 2 hours after irradiation, and then ~5000 cells/events were analyzed by flow cytometry. In some experiments, treated cells were incubated with Nexcelom ViaStain AO/PI staining Solution (catalog#CS2-0106) at room temperature in dark for 20 minutes, and then representative images were captured on a Nikon TE300 fluorescence microscope.

Organotypic tumor spheroids (OTS) model.

Three deidentified fresh human pancreatic tumor surgical specimens were obtained from Tumor Tissue and Pathology Shared Resource at the Wake Forest Baptist Comprehensive Cancer Center (0.8-3g tumor tissue/patient, obtained with informed consent using IRB-approved protocol). OTS was prepared similarly as described by others^{61,62}. In brief, the specimens were minced on ice and strained over 100- μ m filter and 40- μ m filters to generate spheroid fractions (40-100 μ m). Spheroid fractions were resuspended in type I rat tail collagen, and layered on top of 1 ml of pre-reconstructed collagen within a 30 mm, 0.4 mm inner transwell, and then incubated for 1h in a 37°C incubator before added culture medium. Organotypic tumor spheroids (OTS) were cultured for 3-5 days and then treated with medium containing control IgG, α PD-1, α CD73-Dye+ α PD-1, α CD73-Dye+NIR, α CD73-Dye+NIR+ α PD-1, α B7H3-Dye+ α PD-1, α B7H3-Dye+NIR, or α B7H3-Dye+NIR+ α PD-1 combination therapy for 5 days. In some studies, the human CD45⁺ immune cells were identified by FACS with cell lineage markers: DCs (CD11c⁺HLA-DR^{hi}CD1c⁺), M1-like TAM (TAM-M1, CD11b^{hi}CD68⁺CD86⁺), TAM-M2 (CD11b^{hi}CD68⁺CD163⁺), Mo-MDSC (CD11b^{hi}CD14^{hi}), and polymorphonuclear (PMN)-MDSC (CD11b^{hi}CD15^{hi}), B cells (CD19⁺), CD8⁺ T cells (CD3⁺CD8⁺), Treg cells (CD4⁺CD3⁺Foxp3^{hi}), CD4⁺ effector (CD4⁺CD3⁺Foxp3⁻) and NK cells (CD56⁺).

Measurement of NIR cytotoxicity in OTS.

To measure the cytotoxic effect of NIR in OTS, cell death was tested by Nexcelom ViaStain AO/PI staining Solution. Images were captured on a Nikon TE300 fluorescence microscope. Imaging data were analyzed by customized software using Python 3.7 (www.python.org). A strong imaging processing package, opencv-python (<https://pypi.org/project/opencv-python/>) was used to quantify total cell area of each dye (green for live cells or red for dead cells in the figures reported in this manuscript). The steps in our customized software are (1) reading an image into pixels; (2) transforming color of each pixel into colors of green, red, and black, in which intensity for each color (green, red, and black) is scaled from 1 to 255; (3) denoising the colors by setting a threshold for each color intensity. In these analyses, we used $h=150$ for both green (live) and red (dead) colors, i.e. $G_k = \begin{cases} 0, & G_k < h \\ 1, & G_k \geq h \end{cases}$ and

$$R_k = \begin{cases} 0, & R_k < h \\ 1, & R_k \geq h \end{cases}, \text{ where } k \text{ is a pixel } (k = 1, 2, \dots, n), n \text{ is the total number of the pixels in this}$$

image, G_k is the green color intensity of the pixel k , and R_k is the read color intensity of the pixel k ; and (4) calculating relative ratio of live cells as ratio between total number of pixels in green color and red color, $r = \sum_{k=1}^n G_k / (\sum_{k=1}^n G_k + \sum_{k=1}^n R_k)$. Thus, r and $1 - r$ are the output for an image, representing the ratios of the dyed cells, respectively.

In vivo tumor models and treatments.

BALB/c mice were inoculated at the left mammary gland with 5×10^5 4T1.2 or EMT6 or EMT6^{B7H3} or EMT6^{CD73 KO} tumor cells with or without intravenously (i.v.) injection with 1×10^5 4T1.2 or EMT6 or EMT6^{B7H3} or EMT6^{CD73 KO} tumor cells, respectively. Treatments were started on day 5 or 7 when tumors' size reached about 130 mm³. C57BL/6J mice were inoculated subcutaneously (s.c.) at left flank with 2×10^6 Pan02 or Pan02^{B7H3} or Pan02^{OVA}

tumor cells with or without s.c. 0.5×10^6 or 2×10^6 Pan02 or Pan02^{B7H3} or Pan02^{OVA} tumor cells at the right flank. Treatments were started on day 7 when left tumor size reached about 130 mm^3 . Mice were randomized into different groups and mAb-Dye (100 μg) was i.v. injected 1 day before NIR treatment. The tumors on the right flank were exposed once or twice to 690 nm NIR with a total dose of 100 J/cm^2 for each NIR. In some experiments, 150 μg $\alpha\text{PD-1}$ was intraperitoneally (i.p.) injected every three days starting on day 5 or 7 for a total of 4 injections in Pan02, 4T1.2, EMT6 tumor-bearing mice or 5 injections for mice with spontaneous TNBC tumors. All other parts of mice were covered with an aluminum film to avoid light. Mice were monitored daily after treatment. The tumor was measured by caliper and tumor size was calculated as $0.5 \times \text{Length} \times \text{Width}^2$. Mice were euthanized using carbon dioxide and subsequent cervical dislocation.

In vivo Bioluminescence Imaging.

Before imaging, mice were anesthetized with isoflurane and i.p. injected with 100 μL of 20 mg/mL D-Luciferin (Xenogen Corp.). After 8 min, animals were imaged using an IVIS 200 system (Xenogen), according to the manufacturer's instructions. Living Image software (Xenogen) was used to analyze data.

The enzyme-linked immunosorbent spot (ELISpot) assay.

BALB/c mice were inoculated at the left mammary gland with 5×10^5 EMT6 tumor cells and i.v. injection with 1×10^5 EMT6 tumor cells (which allows lung tumor metastasis). IgG, IgG-Dye+NIR, αCD73 -Dye, or αCD73 -Dye+NIR treatments were given on day 5 to orthotopic tumors when the tumor size reached around 130 mm^3 (other parts of mice were shielded from light). The lung metastatic tumor tissues were minced and digested. CD8⁺ T cells in the tissues were isolated by a bead positive selection kit (CD8). Isolated cells per 100 mg tumor tissues were cocultured with irradiated EMT6 tumor cells on IFN γ ELISpot Kit plates (Mouse IFN-gamma ELISpot Kit, R&D Systems) for 48 hours following the manufacturer's instructions. The plates were imaged and evaluated by Cellular Technology Limited ELISPOT Analyzer.

Depletion of NK cells, CD4 T cells, and CD8 T cells.

Anti-NK1.1 (clone: PK136, 200 $\mu\text{g}/\text{mouse}$), or anti-CD4 (clone: GK1.5, 200 $\mu\text{g}/\text{mouse}$), or anti-CD8 (clone: 2.43, 200 $\mu\text{g}/\text{mouse}$) mAbs was i.p. injected every 3 days starting from 1 day before the first NIR treatment^{63,64}.

Extracellular adenosine assay.

Extracellular adenosine assay was performed by using Adenosine Assay Kit (catalog#MET-5090, CELL BIOLABS, INC) according to the manufacturer's instruction. In brief, tumor tissues were harvested after treatments. Tissues were cut into $\sim 2 \times 2 \text{ mm}$ fragments, sonicated in PBS, and centrifuge at $10,000 \times g$ for 10 minutes at 4°C . The supernatant was assayed directly or diluted as necessary in PBS using adenosine assay kit.

Single-cell mass cytometry.

Tumors were dissected, manually dissociated, and digested enzymatically with Collagenase D (Sigma) and DNase I (Roche) in PBS containing 2% FBS for 20 min at room temperature. EDTA was added to a final concentration of 10mM and incubate at room temperature for an additional 5 minutes. The entire suspension was filtered through a 70- μ m cell strainer to obtain a single-cell suspension. Filtered cells were then washed twice and total cell concentrations were determined using an automated cell counter (ThermoFisher) with trypan blue exclusion. Antibodies were either purchased pre-conjugated from Fluidigm or conjugated in-house using Maxpar Antibody Labeling Kit (Fluidigm) according to the manufacturer's instruction. Antibodies include: 89Y-CD45, 141Pr-Ly-6G, 145Nd-CD4, 146Nd-F4/80, 149Sm-CD19, 150Nd-CD24, 151Eu-CD64, 152Sm-CD3e, 153Eu-CD8a, 158Gd-Foxp3, 162Dy-Ly6C, 165Ho-IFN γ , 167Er-Nkp46, 169Tm-CD206, 171Yb-GzmB, 172Yb-CD11b, 174Yb-MHCII, 209Bi-CD11c and 194Pt-Live/Dead. 1×10^6 - 3×10^6 cells per sample were performed by cell staining according to the manufacturer's protocol (Fluidigm). Each antibody was used at manufacturer recommended concentrations. Stained samples were shipped to the CyTOF Core of Dana-Farber Cancer Institute and then analyzed using a CyTOF2. An average of 35,000 CD45⁺ cells (25,000 to 45,000 cells) per sample were evaluated by CyTOF. The CyTOF data were bead-normalized and de-barcoded mass cytometry. We applied Flow-SOM analysis to the CyTOF data. The expression values were arcsinh transformed by the antibodies for transformation. The CD45⁺ immune cells were identified by consensus clustering of the antibodies for cell lineage markers: DCs (CD11c^{hi}MHCII^{hi}CD24⁺), M1-like TAM (TAM-M1, CD11b^{hi}F4/80⁺MHCII^{int/hi}CD206⁻CD24⁻), TAM-M2 (CD11b^{hi}F4/80⁺MHCII^{low/neg}CD206⁺CD24⁻), Mo-MDSC (CD11b^{hi}Ly6C^{hi}Ly6G^{low}), and polymorphonuclear (PMN)-MDSC (CD11b^{hi}Ly6G^{hi}), B cells (CD19⁺), CD8⁺ T cells (CD3⁺CD8⁺), Treg cells (CD3⁺CD4⁺Foxp3⁺), CD4⁺ effector (CD3⁺CD4⁺Foxp3⁻) and NK cells (Nkp46⁺).

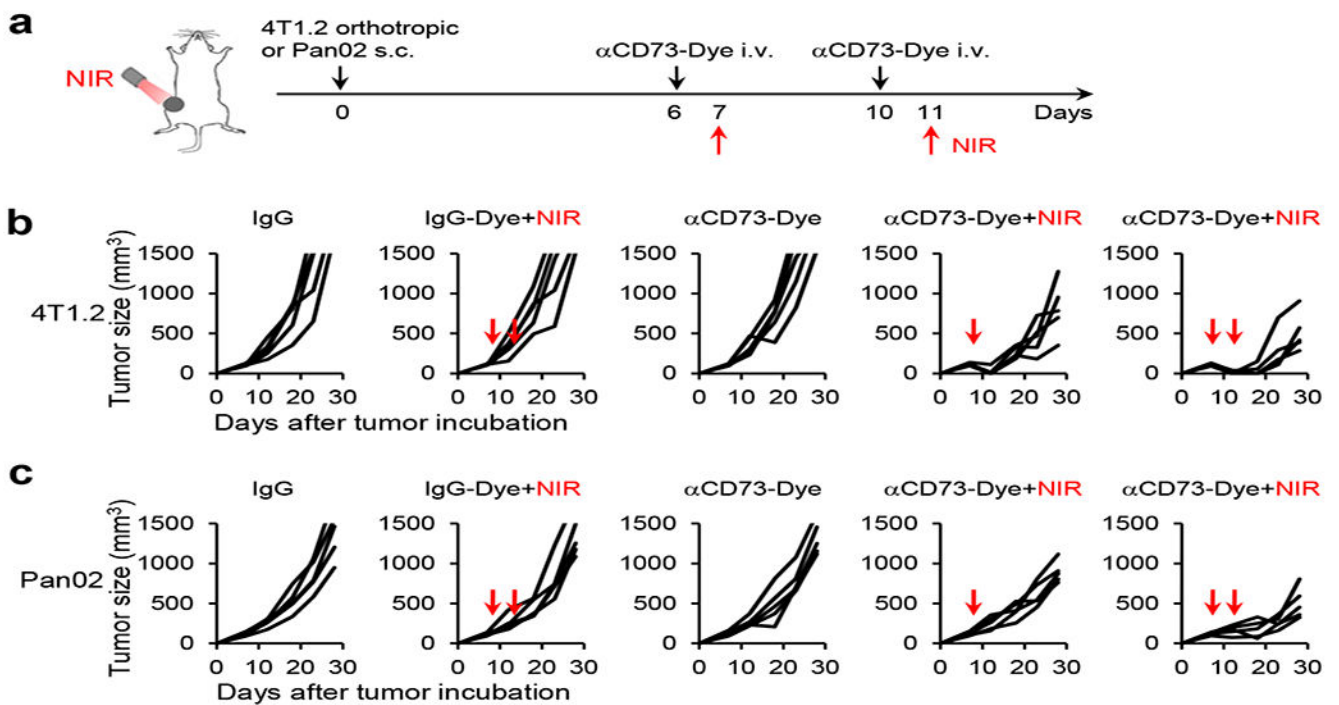
Statistical analyses.

For statistical analysis, Student's *t*-test or ANOVA was used. Survival was analyzed using the log-rank test. A *P*-value less than 0.05 was considered statistically significant. Results are presented as mean \pm standard deviations (SD) unless otherwise indicated.

Reporting Summary.

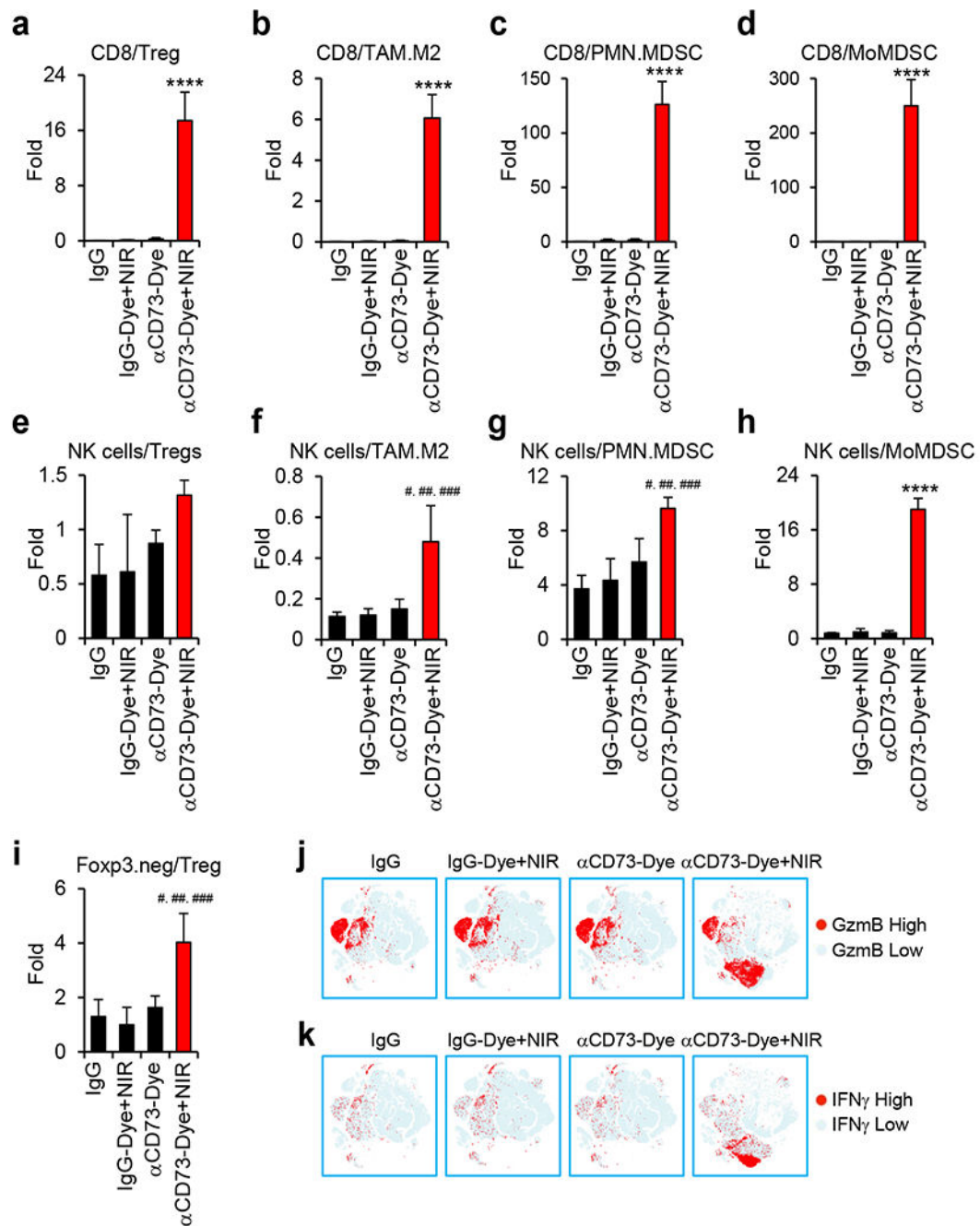
Further information on research design is available in the Nature Research Reporting Summary linked to this article.

Extended Data



ED Fig. 1. α CD73-Dye+NIR treatment shrinks advanced tumors *in vivo*.

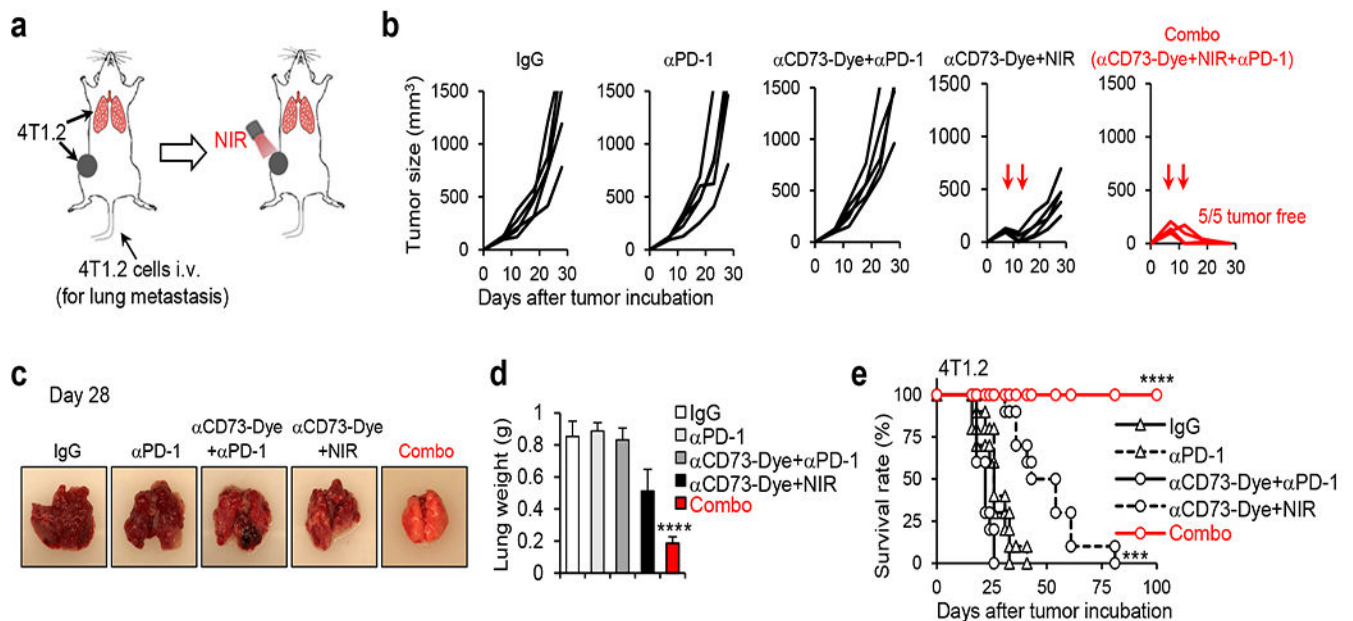
(a) Treatment procedures of α CD73-Dye-mediated NIR irradiation against 4T1.2 and Pan02 tumors *in vivo*. NIR was given on tumors only, while other parts of the mice were shielded from light. Tumor growth curves of 4T1.2 (b) and Pan02 (c) tumors treated with IgG, IgG-Dye+NIR, α CD73-Dye, or α CD73-Dye+NIR ($n=5$ mice/group). The red arrow represents near-infrared (NIR) irradiation. Representative results from one of two repeated experiments are shown.



ED Fig. 2. Changes in ratios of different immune cells in tumors after α CD73-Dye + NIR treatment.

CD8⁺ T cells to Treg cells ratio (a), CD8⁺ T cells to TAM.M2 cells ratio (b), CD8⁺ T cells to PMN.MDSC cells ratio (c), CD8⁺ T cells to Mo.MDSC cells ratio (d), NK cells to Treg cells ratio (e), NK cells to TAM.M2 cells ratio (f), NK cells to PMN.MDSC cells ratio (g), NK cells to Mo.MDSC cells ratio (h), and Foxp3.neg CD4⁺ T cells to Treg cells ratio (i) in 4T1.2 tumors after indicated treatments (as described in Extended Data Figure 1) were tested by CyTOF (n=3 biological replicates). The t-SNE plot of tumor-infiltrating

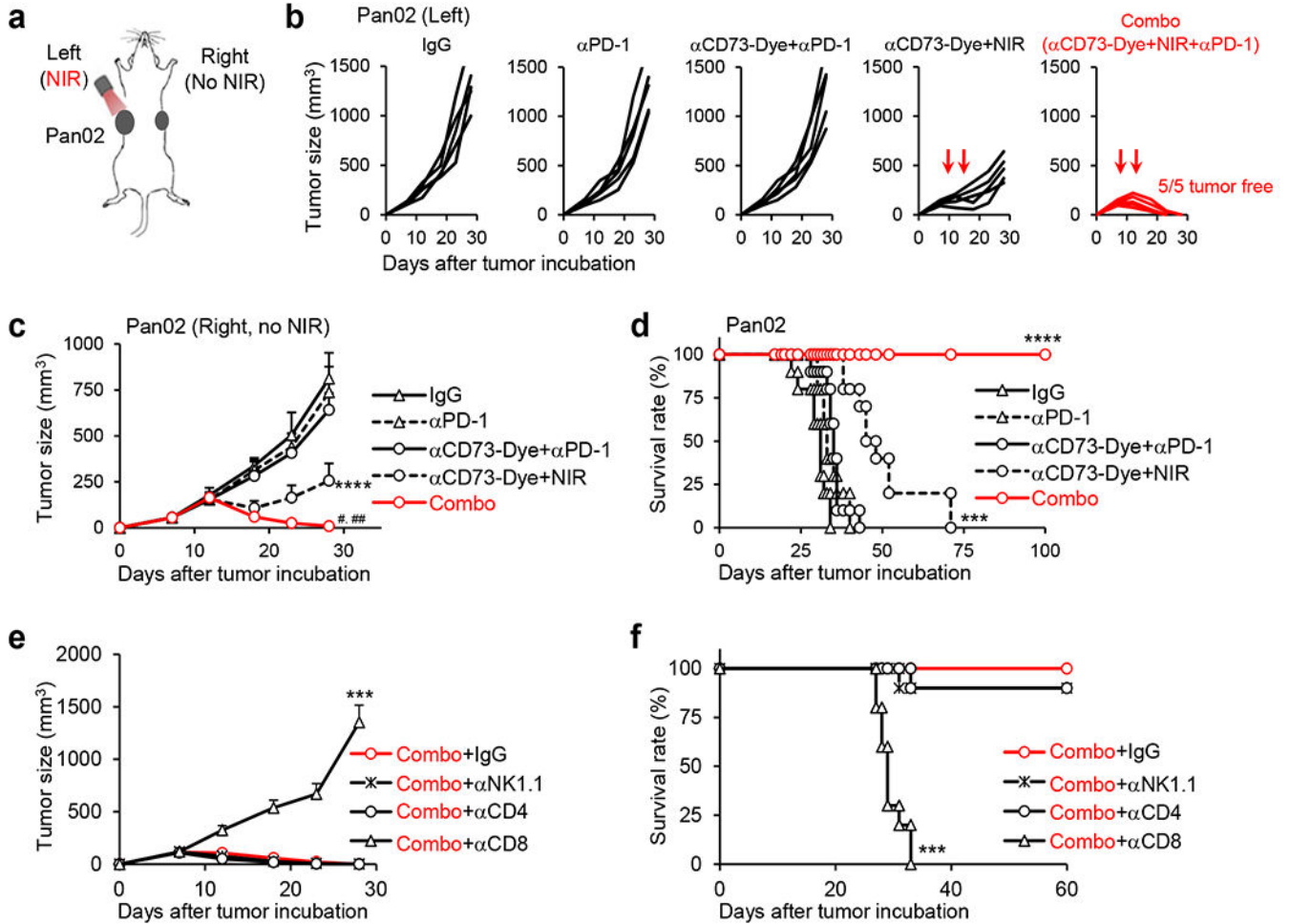
CD45⁺ compartment overlaid with the expression of GzmB (j) and IFN- γ (k) from the 4T1.2 tumor after treatment. Data are mean \pm SD. **** P <0.0001, α CD73-Dye+NIR group compared with IgG, IgG-Dye+NIR, or α CD73-Dye group, one-way ANOVA with Tukey's correction (a, b, c, d, and h). # means ** P = 0.005834, α CD73-Dye+NIR group compared with IgG group, ## means ** P = 0.006561, α CD73-Dye+NIR group compared with IgG-Dye+NIR group, ### means * P =0.010734, α CD73-Dye+NIR group compared with α CD73-Dye group, one-way ANOVA with Tukey's correction (f). # means ** P = 0.002767, α CD73-Dye+NIR group compared with IgG group, ## means ** P = 0.005519, α CD73-Dye+NIR group compared with IgG-Dye+NIR group, ### means * P =0.028222, α CD73-Dye+NIR group compared with α CD73-Dye group, one-way ANOVA with Tukey's correction (g). # means ** P = 0.007576, α CD73-Dye+NIR group compared with IgG group, ## means ** P = 0.004057, α CD73-Dye+NIR group compared with IgG-Dye+NIR group, ### means * P =0.015673, α CD73-Dye+NIR group compared with α CD73-Dye group, one-way ANOVA with Tukey's correction (i).



ED Fig. 3. α CD73-Dye + NIR irradiation synergizes with α PD-1, promoting curative responses in the 4T1.2 tumor model.

(a) Diagram of the treatments. BALB/c mice bearing both orthotopic 4T1.2 tumor (5 × 10⁵ 4T1.2 tumor cells injection in the mammary gland) and lung metastasis tumors (1 × 10⁵ tumor cells injection via tail vein) were treated on day 7 with control IgG, αPD-1, αCD73-Dye+αPD-1, αCD73-Dye+NIR, or αCD73-Dye+NIR+αPD-1 (Combo). NIR irradiation was given on the orthotopic tumor only (other parts of the mice were shielded from light). (b) Tumor growth curves (n=5 mice/group) of the orthotopic 4T1.2 tumors after indicated treatments. (c) Some mice were euthanized on day 28 and representative lung pictures are shown. (d) Summarized lung weight of mice receiving indicated treatments (n=5 biological replicates). (e) Surviving curves of 4T1.2 tumor-bearing mice. Representative results from one of two repeated experiments are shown (n=10 mice/group). Data are mean \pm SD. **** P <0.0001, Combo group compared with IgG, αPD-1, αCD73-Dye+αPD-1, αCD73-Dye+NIR, or αCD73-Dye group.

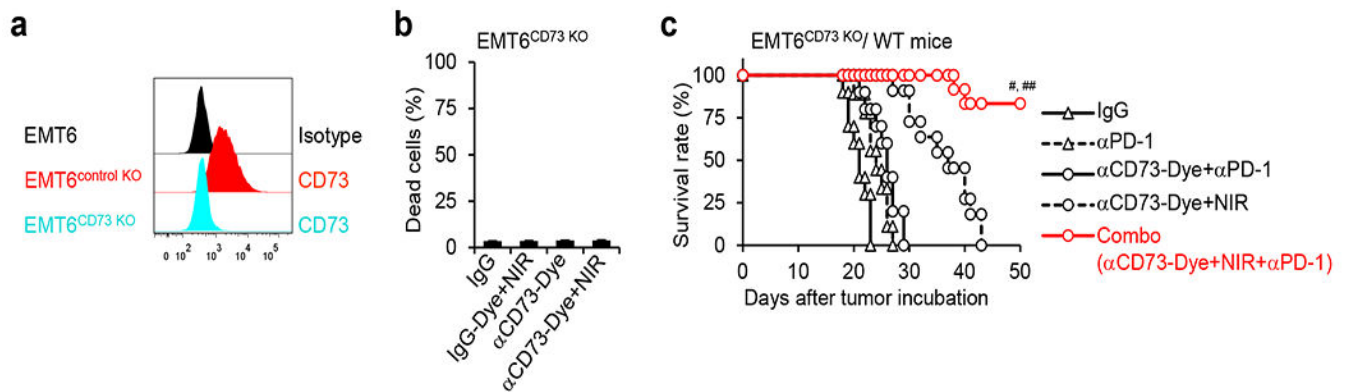
or α CD73-Dye+NIR group, one-way ANOVA with Tukey's correction (d), $***P < 0.001$, α CD73-Dye+NIR group compared with IgG, α PD-1, or α CD73-Dye+ α PD-1 group; $****P < 0.0001$, Combo group compared with IgG, α PD-1, α CD73-Dye+ α PD-1, or α CD73-Dye+NIR group, survival analysis was conducted by log-rank test with holm test for multiple comparisons (e).



ED Fig. 4. α CD73-Dye + NIR + α PD-1 combination treatment induced curative responses in the Pan02 tumor model.

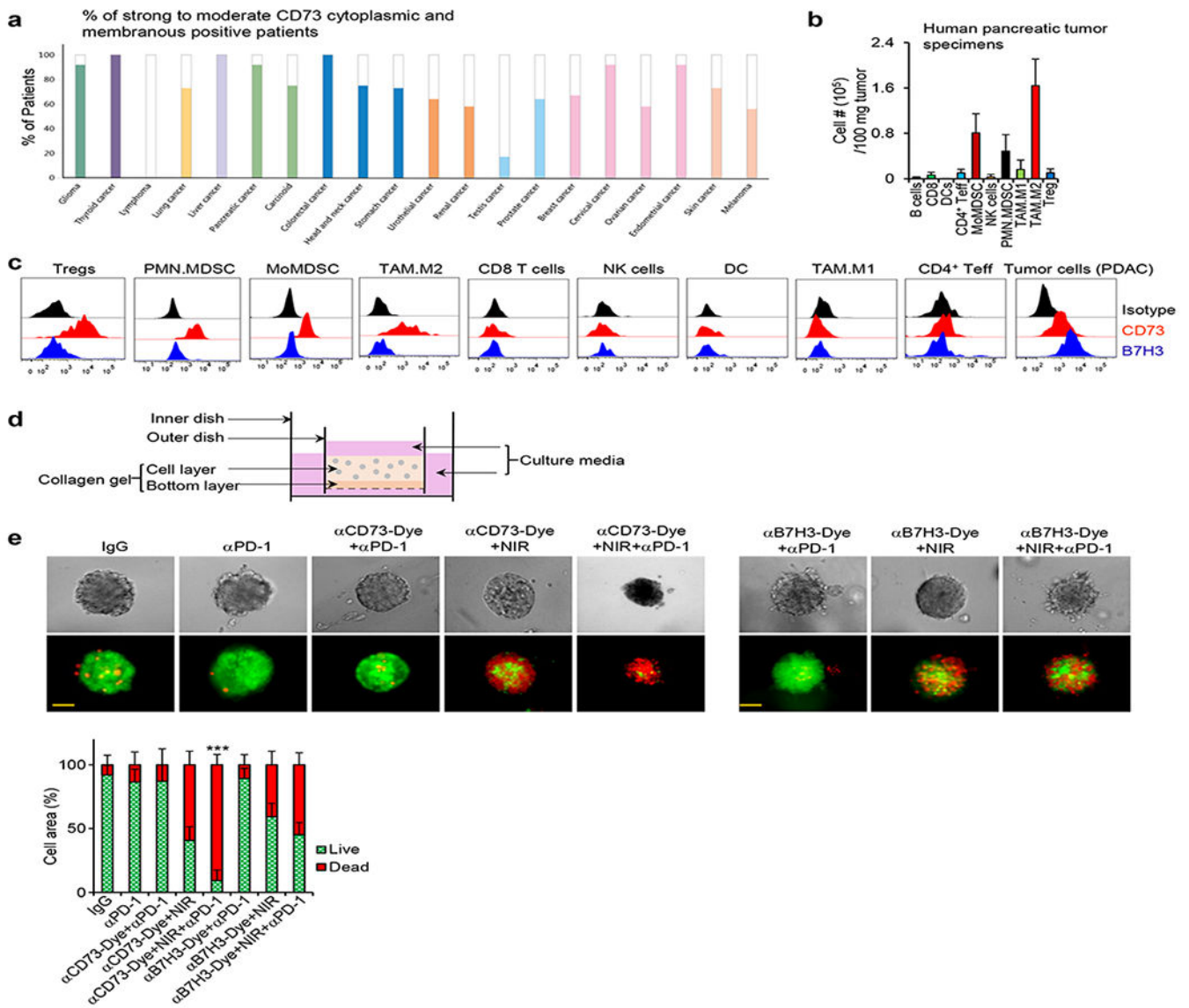
(a) Diagram of the treatments. Pan02 tumor cells were s.c. injected on the left (2×10^6 Pan02 cells) and right (5×10^5 Pan02 cells) flanks of B6 mice, and treated on day 7 with control IgG, α PD-1, α CD73-Dye+ α PD-1, α CD73-Dye+NIR, or α CD73-Dye+NIR+ α PD-1 (Combo). NIR was performed on the left-side tumor only (right-side tumors were shielded from light). (b) Tumor growth curves of NIR-treated left tumors are shown (n=5 mice/group). (c) Tumor growth curves of non-NIR-treated right tumors are shown (n=5 mice/group). (d) Surviving curves of Pan02 tumor-bearing mice (n=10 mice/group). (e) Tumor growth curves and (f) survival curves of Pan02 tumor-bearing mice treated with α CD73-Dye+NIR+ α PD-1 combo therapy together with the depletion of NK cells, CD4⁺ T cells or CD8⁺ T cells. Representative results from one of two repeated experiments are shown.

Data are mean \pm SD. # means **** $P < 0.0001$, α CD73-Dye+NIR group compared with IgG, α PD-1, or α CD73-Dye+ α PD-1 group; # means ** $P = 0.00592$, Combo group compared with α CD73-Dye+NIR group, ## means **** $P < 0.0001$, Combo group compared with IgG, α PD-1, or α CD73-Dye+ α PD-1 group, two-way ANOVA with Holm–Sidak test for multiple comparisons (c). *** $P < 0.001$, α CD73-Dye+NIR group compared with IgG, α PD-1, or α CD73-Dye+ α PD-1 group, **** $P < 0.0001$, Combo group compared with IgG, α PD-1, α CD73-Dye+ α PD-1, or α CD73-Dye+NIR group, survival analysis was conducted by log-rank test with holm test for multiple comparisons (d). *** $P < 0.001$, Combo+ α CD8 group compared with Combo+IgG, Combo+ α NK1.1, or Combo+ α CD4 group, two-way ANOVA with Holm–Sidak test for multiple comparisons (e). *** $P < 0.001$, Combo+ α CD8 group compared with Combo+IgG, Combo+ α NK1.1, or Combo+ α CD4 group, survival analysis was conducted by log-rank test with holm test for multiple comparisons (f).



ED Fig. 5. Effects of α CD73-Dye + NIR + α PD-1 combination treatment in the EMT6^{CD73} KO tumor model.

(a) FACS analysis for surface expression of CD73 in EMT6 CD73 knockout (EMT6^{CD73} KO) cells. (b) EMT6^{CD73} KO cells were treated as indicated *in vitro*. The percentage of dead cells was determined by FACS after PI staining (n=3 biological replicates). (c) BALB/c mice bearing both orthotopic EMT6^{CD73} KO tumor (5×10^5 EMT6^{CD73} KO tumor cells injection in the mammary gland) and lung metastasis tumors (1×10^5 EMT6^{CD73} KO tumor cells injection via tail vein) were treated on day 5 with control IgG, α PD-1, α CD73-Dye+ α PD-1, α CD73-Dye+NIR, or α CD73-Dye+NIR+ α PD-1 (Combo). NIR irradiation was given on the orthotopic tumor only (other parts of the mice were shielded from light). Mice survival curves (n=9/ α PD-1 group, n=11/ α CD73-Dye+NIR group, n=12/Combo group, n=10/other groups) are shown. Representative results from one of two repeated experiments are shown. Data are mean \pm SD. # mean ** $P = 0.00114439$, Combo group compared with α CD73-Dye+NIR group; ## means *** $P < 0.001$, Combo group compared with IgG, α PD-1, or α CD73-Dye+ α PD-1 group, survival analysis was conducted by log-rank test with holm test for multiple comparisons (c).



ED Fig. 6. Effects of α CD73-Dye + NIR + α PD-1 combination therapy in human pancreatic cancer.

(a) CD73 protein levels in the HPA dataset. Most cancer tissues displayed strong to moderate membranous and cytoplasmic CD73 positivity. Lymphomas and testicular cancers showed weak positivity or were negative. (b) Cell number per 100 mg tumor tissue of indicated immune cell subsets were determined by FACS (n=3). (c) FACS analysis for surface expression of CD73 or B7H3 on cells isolated from pancreatic tumor specimens. Representative data are shown. (d) Diagram of organotypic tumor spheroids (OTS), modified from a published study⁶². (e) Human PDAC OTS were treated as indicated *ex vivo*. Cell death was tested by Nexcelom ViaStain AO/PI staining Solution. Green represents live cells; red represents dead cells. Orange bar: 50 μ m. Representative data and summarized results are shown, n=8/group (2-3 OTS from each patient for each indicated treatment; and OTS from 3 patients were used). Data are mean \pm SD. *** P <0.001, α CD73-

Dye+NIR+αPD-1 group compared with any other groups, one-way ANOVA with Tukey's correction (e).

Supplementary Material

Refer to Web version on PubMed Central for supplementary material.

Acknowledgements

This work was supported by grants from the National Cancer Institute (NCI, 4R00CA190910-03; 1R37CA251318-01; 1R01CA248111-01A1; R01 CA258477-01; 1R01CA264102-01), NCI P30 Administrative Supplement for Cell-Based Therapy (3P30CA012197-44S5), Daryl and Marguerite Errett Discovery Award 2020, ACS Research Scholar Grant (RSG-19-149-01-LIB), Wake Forest Baptist Comprehensive Cancer Center (WFBCCC) Push Pilot projects and CPRIT Scholar (RR210067). Research reported in this publication was also supported by the National Center for Advancing Translational Sciences of the National Institutes of Health under Award Number UL1TR001420 (CTSI Pilot Grant Award 2018, CTSI Pilot Grant Award 2019, and CTSI Ignition Fund Pilot award). The authors wish to thank Indra M. Newman, Ph.D. from the Wake Forest CTSI, for manuscript editing assistance. This study was also supported by the National Cancer Institute's Cancer Center Support Grant award number P30CA012197 issued to the Wake Forest Baptist Comprehensive Cancer Center. The content is solely the responsibility of the authors and does not necessarily represent the official views of the National Cancer Institute.

Data availability

The main data supporting the results in this study are available within the paper and its Supplementary Information. Source data for the figures are provided in this paper. The raw and analysed datasets generated during the study are too large to be publicly shared, yet they are available for research purposes from the corresponding author on reasonable request.

References

1. Reck M et al. Pembrolizumab versus Chemotherapy for PD-L1-Positive Non-Small-Cell Lung Cancer. *N. Engl. J. Med* 375, 1823–1833 (2016). [PubMed: 27718847]
2. Hodi FS et al. Improved survival with ipilimumab in patients with metastatic melanoma. *N. Engl. J. Med* 363, 711–23 (2010). [PubMed: 20525992]
3. Adams S et al. Phase 2 study of pembrolizumab (pembro) monotherapy for previously treated metastatic triple-negative breast cancer (mTNBC): KEYNOTE-086 cohort A. *ASCO 1008* (2017). doi:J Clin Oncol 2017;35
4. Vonderheide RH et al. Tremelimumab in combination with exemestane in patients with advanced breast cancer and treatment-associated modulation of inducible costimulator expression on patient T cells. *Clin. Cancer Res* 16, 3485–3494 (2010). [PubMed: 20479064]
5. Patnaik A et al. Phase i study of pembrolizumab (MK-3475; Anti-PD-1 monoclonal antibody) in patients with advanced solid tumors. *Clin. Cancer Res* 21, 4286–4293 (2015). [PubMed: 25977344]
6. Brahmer JR et al. Safety and Activity of Anti-PD-L1 Antibody in Patients with Advanced Cancer. *N. Engl. J. Med* 366, 2455–2465 (2012). [PubMed: 22658128]
7. Segal N et al. Preliminary data from a multi-arm expansion study of MEDI4736, an anti-PD-L1 antibody. | 2014 ASCO Annual Meeting | Abstracts | Meeting Library. *Journal of Clinical Oncology* 32:5s, 2014 (suppl; abstr 3002[^]) (2014). doi:10.1200/jco.2014.32.15_suppl.3002
8. Royal RE et al. Phase 2 trial of single agent ipilimumab (Anti-CTLA-4) for locally advanced or metastatic pancreatic adenocarcinoma. *J. Immunother* 33, 828–833 (2010). [PubMed: 20842054]
9. Sharma P, Hu-Lieskovan S, Wargo JA & Ribas A Primary, Adaptive, and Acquired Resistance to Cancer Immunotherapy. *Cell* 168, 707–723 (2017). [PubMed: 28187290]
10. Granier C et al. Mechanisms of action and rationale for the use of checkpoint inhibitors in cancer. *ESMO Open* 2, e000213 (2017). [PubMed: 28761757]

11. Bjoern J et al. Immunological correlates of treatment and response in stage IV malignant melanoma patients treated with Ipilimumab. *Oncoimmunology* 5, (2016).
12. Holmgaard RB, Zamarin D, Lesokhin A, Merghoub T & Wolchok JD Targeting myeloid-derived suppressor cells with colony stimulating factor-1 receptor blockade can reverse immune resistance to immunotherapy in indoleamine 2,3-dioxygenase-expressing tumors. *EBioMedicine* 6, 50–58 (2016). [PubMed: 27211548]
13. Meyer C et al. Frequencies of circulating MDSC correlate with clinical outcome of melanoma patients treated with ipilimumab. *Cancer Immunol. Immunother* 63, 247–257 (2014). [PubMed: 24357148]
14. Highfill SL et al. Disruption of CXCR2-mediated MDSC tumor trafficking enhances anti-PD1 efficacy. *Sci. Transl. Med* 6, (2014).
15. Gebhardt C et al. Myeloid Cells and Related Chronic Inflammatory Factors as Novel Predictive Markers in Melanoma Treatment with Ipilimumab. *Clin. Cancer Res* 21, 5453–9 (2015). [PubMed: 26289067]
16. Diaz-Montero CM, Finke J & Montero AJ Myeloid-derived suppressor cells in cancer: Therapeutic, predictive, and prognostic implications. *Semin. Oncol* 41, 174–184 (2014). [PubMed: 24787291]
17. Kumar V, Patel S, Tcyganov E & Gabrilovich DI The Nature of Myeloid-Derived Suppressor Cells in the Tumor Microenvironment. *Trends in Immunology* 37, 208–220 (2016). [PubMed: 26858199]
18. Talmadge JE & Gabrilovich DI History of myeloid-derived suppressor cells. *Nat Rev Cancer* 13, 739–752 (2013). [PubMed: 24060865]
19. Colombo MP & Piconese S Regulatory T-cell inhibition versus depletion: The right choice in cancer immunotherapy. *Nature Reviews Cancer* 7, 880–887 (2007). [PubMed: 17957190]
20. Nishikawa H & Sakaguchi S Regulatory T cells in cancer immunotherapy. *Current Opinion in Immunology* 27, 1–7 (2014). [PubMed: 24413387]
21. Buckner JH Mechanisms of impaired regulation by CD4+CD25+FOXP3+ regulatory T cells in human autoimmune diseases. *Nat. Rev. Immunol* 10, 849–859 (2010). [PubMed: 21107346]
22. Sato K, Nagaya T, Mitsunaga M, Choyke PL & Kobayashi H Near infrared photoimmunotherapy for lung metastases. *Cancer Lett.* 365, 112–121 (2015). [PubMed: 26021765]
23. Mitsunaga M et al. Cancer cell-selective in vivo near infrared photoimmunotherapy targeting specific membrane molecules. *Nat. Med* 17, 1685–1691 (2011). [PubMed: 22057348]
24. Sato K et al. Spatially selective depletion of tumor-associated regulatory T cells with near-infrared photoimmunotherapy. *Sci. Transl. Med* 8, (2016).
25. Mellman I, Coukos G & Dranoff G Cancer immunotherapy comes of age. *Nature* (2011). doi:10.1038/nature10673
26. Li P et al. BATF-JUN is critical for IRF4-mediated transcription in T cells. *Nature* (2012). doi:10.1038/nature11530
27. Elpek KG et al. The tumor microenvironment shapes lineage, transcriptional, and functional diversity of infiltrating myeloid cells. *Cancer Immunol. Res* (2014). doi:10.1158/2326-6066.CIR-13-0209
28. Tuit S et al. Transcriptional Signature Derived from Murine Tumor-Associated Macrophages Correlates with Poor Outcome in Breast Cancer Patients. *Cell Rep.* (2019). doi:10.1016/j.celrep.2019.09.067
29. Azambuja JH et al. Blockade of CD73 delays glioblastoma growth by modulating the immune environment. *Cancer Immunol. Immunother* (2020). doi:10.1007/s00262-020-02569-w
30. Goswami S et al. Immune profiling of human tumors identifies CD73 as a combinatorial target in glioblastoma. *Nature Medicine* (2020). doi:10.1038/s41591-019-0694-x
31. Beavis PA, Stagg J, Darcy PK & Smyth MJ CD73: A potent suppressor of antitumor immune responses. *Trends in Immunology* 33, 231–237 (2012). [PubMed: 22487321]
32. Buisseret L et al. Clinical significance of CD73 in triple-negative breast cancer: Multiplex analysis of a phase III clinical trial. *Ann. Oncol* (2018). doi:10.1093/annonc/mdx730

33. Azad A et al. PD-L1 blockade enhances response of pancreatic ductal adenocarcinoma to radiotherapy. *EMBO Mol. Med* 9, 167–180 (2017). [PubMed: 27932443]
34. Corbett TH et al. Induction and Chemotherapeutic Response of Two Transplantable Ductal Adenocarcinomas of the Pancreas in C57BL/6 Mice. *Cancer Res.* 44, 717–726 (1984). [PubMed: 6692374]
35. Allard B, Pommey S, Smyth MJ & Stagg J Targeting CD73 enhances the antitumor activity of anti-PD-1 and anti-CTLA-4 mAbs. *Clin. Cancer Res* (2013). doi:10.1158/1078-0432.CCR-13-0545
36. Stagg J et al. Anti-CD73 antibody therapy inhibits breast tumor growth and metastasis. *Proc. Natl. Acad. Sci. U. S. A* (2010). doi:10.1073/pnas.0908801107
37. de Mingo Pulido Á et al. TIM-3 Regulates CD103+ Dendritic Cell Function and Response to Chemotherapy in Breast Cancer. *Cancer Cell* (2018). doi:10.1016/j.ccell.2017.11.019
38. Lin EY et al. Progression to Malignancy in the Polyoma Middle T Oncoprotein Mouse Breast Cancer Model Provides a Reliable Model for Human Diseases. *Am. J. Pathol* 163, 2113–2126 (2003). [PubMed: 14578209]
39. Guy CT, Cardiff RD & Muller WJ Induction of mammary tumors by expression of polyomavirus middle T oncogene: a transgenic mouse model for metastatic disease. *Mol. Cell. Biol* 12, 954–961 (1992). [PubMed: 1312220]
40. Uhlen M et al. Tissue-based map of the human proteome. *Science* (80-.). 347, 1260419–1260419 (2015).
41. Bedard PL, Hansen AR, Ratain MJ & Siu LL Tumour heterogeneity in the clinic. *Nature* 501, 355–364 (2013). [PubMed: 24048068]
42. Agarwal R & Kaye SB Ovarian cancer: Strategies for overcoming resistance to chemotherapy. *Nature Reviews Cancer* 3, 502–516 (2003). [PubMed: 12835670]
43. Lackner MR, Wilson TR & Settleman J Mechanisms of acquired resistance to targeted cancer therapies. *Future Oncology* 8, 999–1014 (2012). [PubMed: 22894672]
44. Neel DS & Bivona TG Resistance is futile: overcoming resistance to targeted therapies in lung adenocarcinoma. *npj Precis. Oncol* 1, 3 (2017). [PubMed: 29152593]
45. Vijayan D, Young A, Teng MWL & Smyth MJ Targeting immunosuppressive adenosine in cancer. *Nat. Rev. Cancer* 17, 709–724 (2017). [PubMed: 29059149]
46. Chen S et al. CD73 expression on effector T cells sustained by TGF- β facilitates tumor resistance to anti-4–1BB/CD137 therapy. *Nat. Commun* (2019). doi:10.1038/s41467-018-08123-8
47. De Leve S, Wirsdörfer F & Jendrossek V Targeting the immunomodulatory CD73/adenosine system to improve the therapeutic gain of radiotherapy. *Frontiers in Immunology* (2019). doi:10.3389/fimmu.2019.00698
48. Zhang B CD73: A novel target for cancer immunotherapy. *Cancer Research* (2010). doi:10.1158/0008-5472.CAN-10-1544
49. Leone RD & Emens LA Targeting adenosine for cancer immunotherapy. *Journal for ImmunoTherapy of Cancer* (2018). doi:10.1186/s40425-018-0360-8
50. Mixed Reviews for A2AR Inhibitor in NSCLC. *Cancer discovery* 9, OF2 (2019).
51. Narravula S, Lennon PF, Mueller BU & Colgan SP Regulation of Endothelial CD73 by Adenosine: Paracrine Pathway for Enhanced Endothelial Barrier Function. *J. Immunol* (2000). doi:10.4049/jimmunol.165.9.5262
52. Yu M et al. CD73 on cancer-associated fibroblasts enhanced by the A2B-mediated feedforward circuit enforces an immune checkpoint. *Nat. Commun* (2020). doi:10.1038/s41467-019-14060-x
53. Seaman S et al. Eradication of Tumors through Simultaneous Ablation of CD276/B7-H3-Positive Tumor Cells and Tumor Vasculature. *Cancer Cell* 31, 501–515.e8 (2017). [PubMed: 28399408]
54. Keen JC & Moore HM The genotype-tissue expression (GTEx) project: Linking clinical data with molecular analysis to advance personalized medicine. *J. Pers. Med* 5, 22–29 (2015). [PubMed: 25809799]
55. Yu NYL et al. Complementing tissue characterization by integrating transcriptome profiling from the human protein atlas and from the FANTOM5 consortium. *Nucleic Acids Res.* 43, 6787–6798 (2015). [PubMed: 26117540]

56. Sciarra A et al. CD73 expression in normal and pathological human hepatobiliopancreatic tissues. *Cancer Immunol. Immunother* (2019). doi:10.1007/s00262-018-2290-1
57. Bown SG et al. Photodynamic therapy for cancer of the pancreas. *Gut* 50, 549–57 (2002). [PubMed: 11889078]
58. Xue G, Jin G, Fang J & Lu Y IL-4 together with IL-1 β induces antitumor Th9 cell differentiation in the absence of TGF- β signaling. *Nat. Commun* 10, 1376 (2019). [PubMed: 30914642]
59. Brinke A Ten et al. Monitoring T-cell responses in translational studies: Optimization of dye-based proliferation assay for evaluation of antigen-specific responses. *Front. Immunol* (2017). doi:10.3389/fimmu.2017.01870
60. Mao C, Li F, Zhao Y, Debinski W & Ming X P-glycoprotein-targeted photodynamic therapy boosts cancer nanomedicine by priming tumor microenvironment. *Theranostics* (2018). doi:10.7150/thno.29580
61. Jenkins RW et al. Ex vivo profiling of PD-1 blockade using organotypic tumor spheroids. *Cancer Discov.* 8, 196–215 (2018). [PubMed: 29101162]
62. Ootani A et al. Sustained in vitro intestinal epithelial culture within a Wnt-dependent stem cell niche. *Nat. Med* (2009). doi:10.1038/nm.1951
63. Lu Y et al. Th9 cells promote antitumor immune responses in vivo. *J. Clin. Invest* 122, 4160–4171 (2012). [PubMed: 23064366]
64. Lu Y et al. Th9 Cells Represent a Unique Subset of CD4+ T Cells Endowed with the Ability to Eradicate Advanced Tumors. *Cancer Cell* 33, 1048–1060.e7 (2018). [PubMed: 29894691]

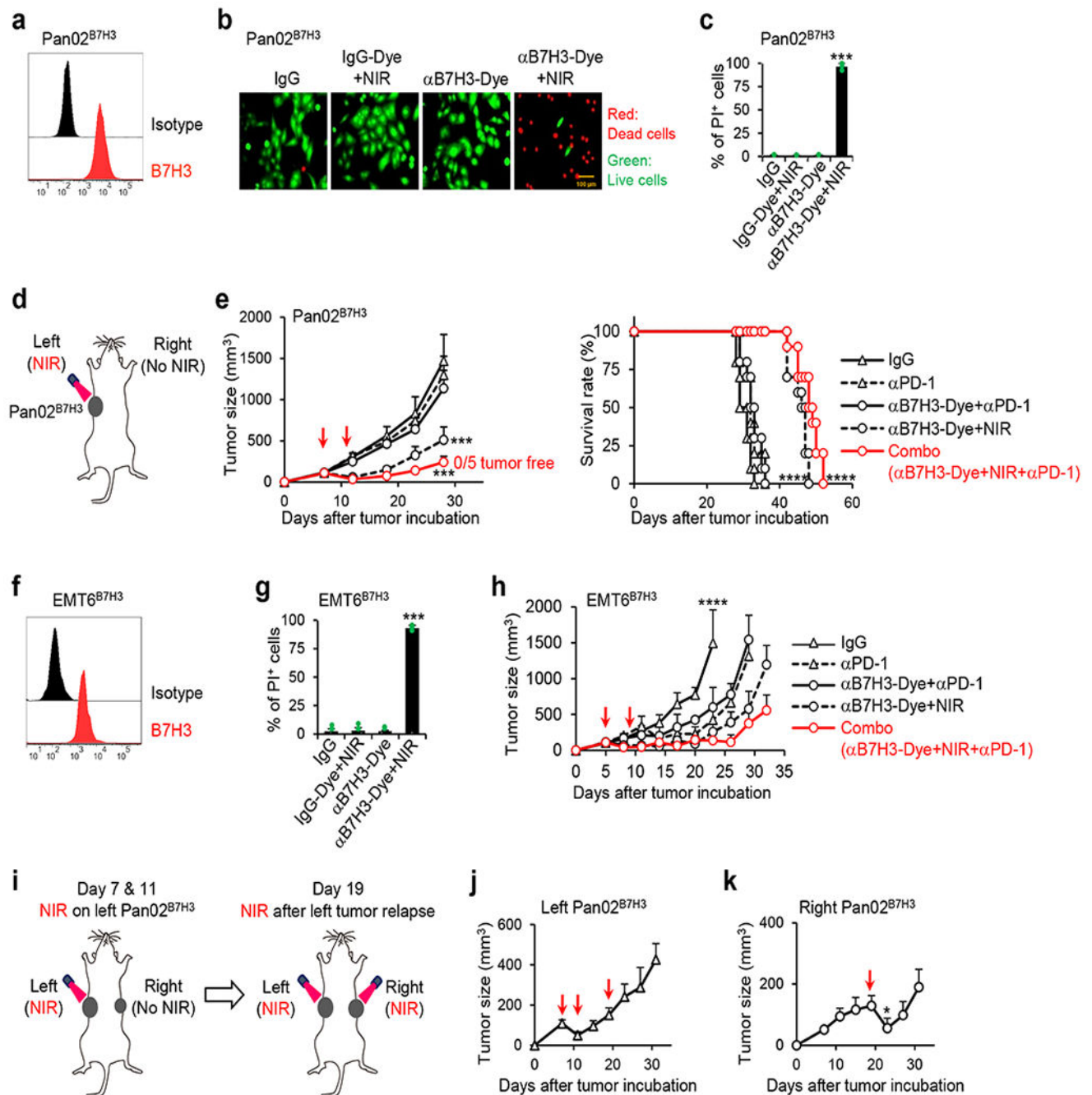


Fig. 1 | Relapse of resistant tumors is inevitable when merely targeting tumor-expressed antigen.

(a) The surface expression of B7H3 on Pan02^{B7H3} cancer cells was assessed by FACS. (b) Pan02^{B7H3} cancer cells were treated with IgG, IgG-Dye+NIR, αB7H3-Dye, or αB7H3-Dye+NIR *in vitro*. Cell death was tested by Nexcelom ViaStain AO/PI staining Solution. Green represents live cells; red represents dead cells. Representative images are shown. (c) The percentage of PI⁺ cells was tested by FACS (n=3 biological replicates). (d) Diagram of the treatments. Pan02^{B7H3} tumor cells were s.c. injected on the left (2×10⁶ Pan02^{B7H3} cells) flanks of B6 mice, and treated on day 7 and day 11 with control IgG, αPD-1,

α B7H3-Dye+ α PD-1, α B7H3-Dye+NIR, or α B7H3-Dye+NIR+ α PD-1 (Combo). NIR was performed on the left-side tumor only (other parts of the mice were shielded from light). (e) Tumor responses and survival curves are shown (total # of mice/group=10). (f) The surface expression of B7H3 on EMT6^{B7H3} cancer cells was assessed by FACS. (g) EMT6^{B7H3} cells were treated as indicated *in vitro*. The percentage of dead cells was determined by FACS after PI staining (n=3 biological replicates). (h) BALB/c mice bearing both orthotopic EMT6^{B7H3} tumor (5×10^5 EMT6^{B7H3} tumor cells injection in the mammary gland) and lung metastasis tumors (1×10^5 EMT6^{B7H3} tumor cells injection via tail vein) were treated on day 5 with control IgG, α PD-1, α B7H3-Dye+ α PD-1, α B7H3-Dye+NIR, or α B7H3-Dye+NIR+ α PD-1 (Combo). NIR irradiation was given on the orthotopic tumor only (other parts of the mice were shielded from light). Orthotopic tumor growth curves (n=5 mice/group) are shown. (i) Diagram of the treatments. Pan02^{B7H3} tumor cells were s.c. injected on the left (2×10^6 Pan02^{B7H3} cells) and right (5×10^5 Pan02^{B7H3} cells) flanks of B6 mice, and treated on day 7 and day 11 with α B7H3-Dye+NIR+ α PD-1 on the left-side tumor only (right-side tumors were shielded from light; α B7H3-Dye injected i.v.). Mice were treated with α B7H3-Dye+NIR again for both left and right tumors on day 19 when left tumors recurred. (j) Tumor responses of left-side tumors are shown (n=5 mice/group). (k) Tumor responses of right-side tumors are shown (n=5 mice/group). (IgG-Dye represents IR-700 dye-conjugated IgG, α B7H3-Dye represents IR-700 dye-conjugated anti-B7H3 mAbs. Red arrow represents red-to-near-infrared (NIR) irradiation). Representative results from one of two repeated experiments are shown. Data are mean \pm SD. *** $P < 0.001$, α B7H3-Dye+NIR group compared with IgG, IgG-Dye+NIR, or α B7H3-Dye group, one-way ANOVA with Tukey's correction (c and g). *** $P < 0.001$, α B7H3-Dye+NIR or Combo group compared with IgG, α PD-1, or α B7H3-Dye+ α PD-1 group, two-way ANOVA with Holm-Sidak test for multiple comparisons (e). **** $P < 0.0001$, α B7H3-Dye+NIR or Combo group compared with IgG, α PD-1, or α B7H3-Dye+ α PD-1 group, survival analysis was conducted by log-rank test with holm test for multiple comparisons (e). **** $P < 0.0001$, IgG group compared with α PD-1, α B7H3-Dye+ α PD-1, α B7H3-Dye+NIR, or Combo group, two-way ANOVA with Holm-Sidak test for multiple comparisons (h). * $P = 0.015$, compared with day 19, two-way ANOVA with Holm-Sidak test for multiple comparisons (k).

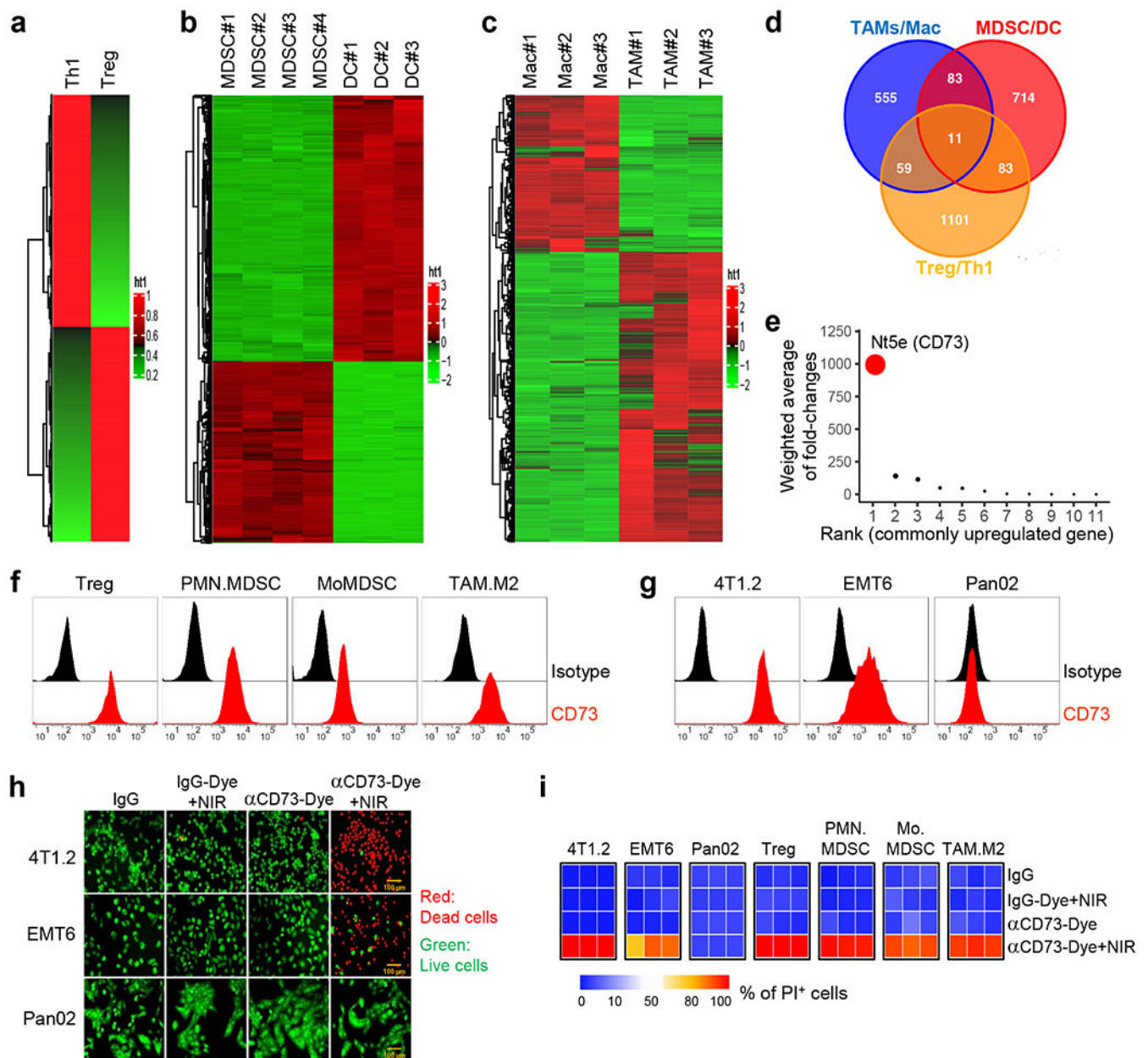


Fig. 2 | Targeting CD73 specifically kills cancer cells and all major types of immunosuppressive cells.

(a) Hierarchical clustering of gene expression of Treg cells and Th1 cells. (b) Hierarchical clustering of gene expression of MDSCs and DCs. (c) Hierarchical clustering of gene expression of TAM.M2 cells and tissue macrophages. (d) Venn diagrams displaying the number of upregulated genes of Treg cells, MDSCs, and TAM.M2 cells. (e) Rank-adjusted fold-change analysis for 11 commonly upregulated genes among Treg cells, MDSCs, and TAM.M2 cells. (f) Surface expression levels of CD73 on Treg cells, PMN.MDSC, MoMDSC, and TAM.M2 cells isolated from EMT6 tumors. (g) Surface expression levels of CD73 on 4T1.2, EMT6, and Pan02 cancer cells were assessed by FACS. (h) 4T1.2, EMT6, and Pan02 cancer cells were treated with IgG, IgG-Dye+NIR, α CD73-Dye, or α CD73-Dye+NIR.

Dye+NIR *in vitro*. Cell death was tested by Nexcelom ViaStain AO/PI staining Solution. Green represents live cells; red represents dead cells. Representative images are shown. (i) Cell necrosis of tumor cells and Treg cells, PMN.MDSC, MoMDSC, and TAM.M2 cells isolated from EMT6 tumors. Cells were treated by IgG, IgG-Dye+NIR, α CD73-Dye, or α CD73-Dye+NIR *in vitro*. Shown is the heatmap illustrating the percentage of PI⁺ dead cells tested by FACS. Representative results from one of two repeated experiments are shown.

Author Manuscript

Author Manuscript

Author Manuscript

Author Manuscript

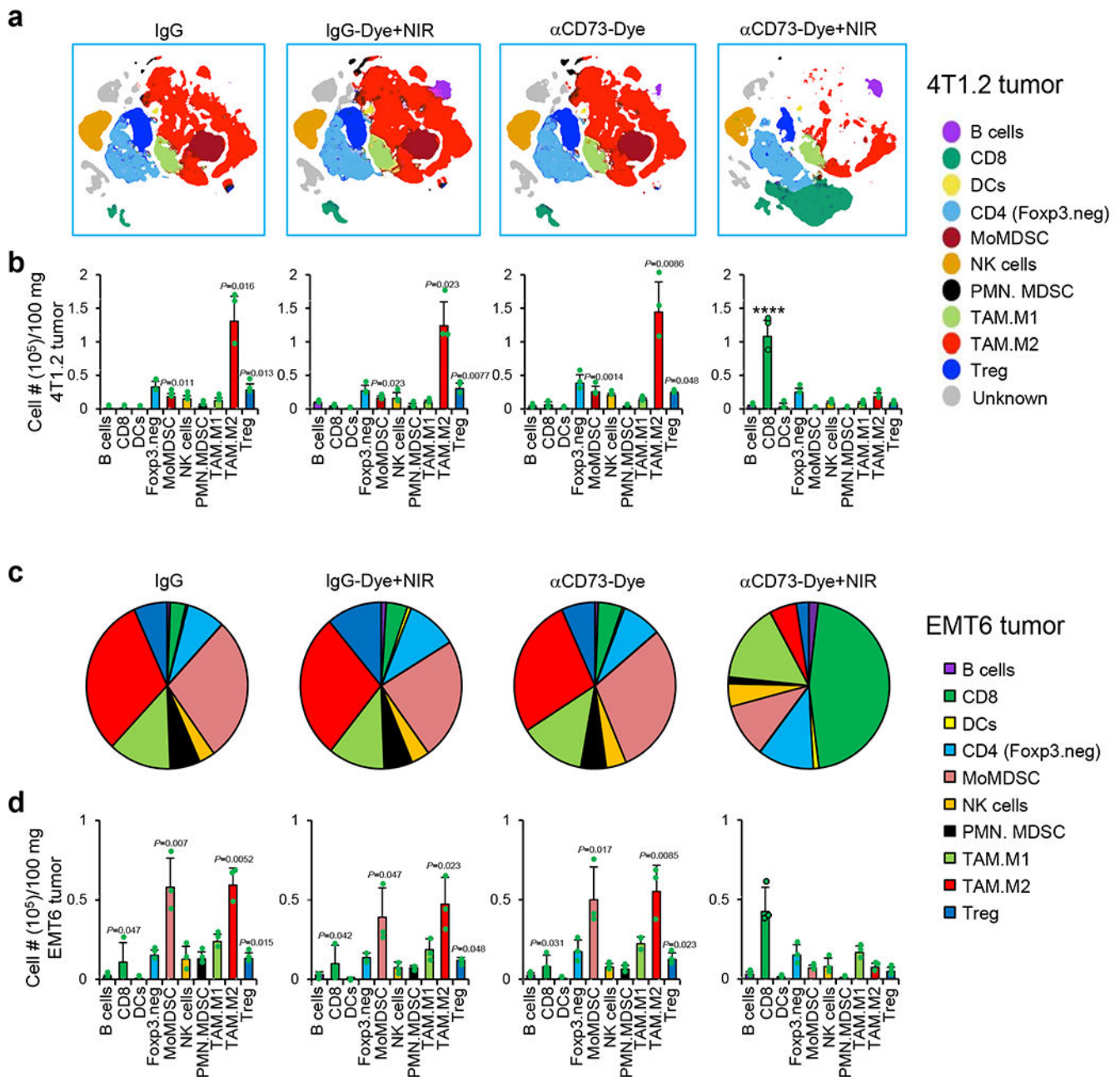


Fig. 3 | Targeting CD73⁺ cells modifies the tumor immune landscape and bolsters CTL responses *in vivo*.

4T1.2 and EMT6 tumor-bearing mice were treated with IgG, IgG-Dye+NIR, α CD73-Dye, or α CD73-Dye+NIR (mice were treated similarly as shown in Extended Data Fig. 1b).

Tumors were harvest 2 hours after the treatment. (a) The t-SNE plot of 4T1.2 tumor-infiltrating CD45⁺ compartment overlaid with color-coded clusters from the treated mice.

CytoFACS was used to detect cell subsets in tumor tissues combined from 3–4 tumors of the same treatment group. (b) Calculated cell numbers per 100 mg 4T1.2 tumor are shown by indicated immune cell subsets (n=3 biological replicates).

(c) Percentage of EMT6 tumor-infiltrating CD45⁺ immune cell subsets from the treated tumor-bearing mice. FACS

was used to detect cell subsets in tumor tissues. **(d)** Calculated cell numbers per 100 mg EMT6 tumor are shown by indicated immune cell subsets (n=3 biological replicates). Representative results from one of two repeated experiments are shown. Data are mean \pm SD. **** $P < 0.0001$, α CD73-Dye+NIR group compared with IgG, IgG-Dye+NIR, or α CD73-Dye group, one-way ANOVA with Holm–Sidak test for multiple comparisons **(b, d)**.

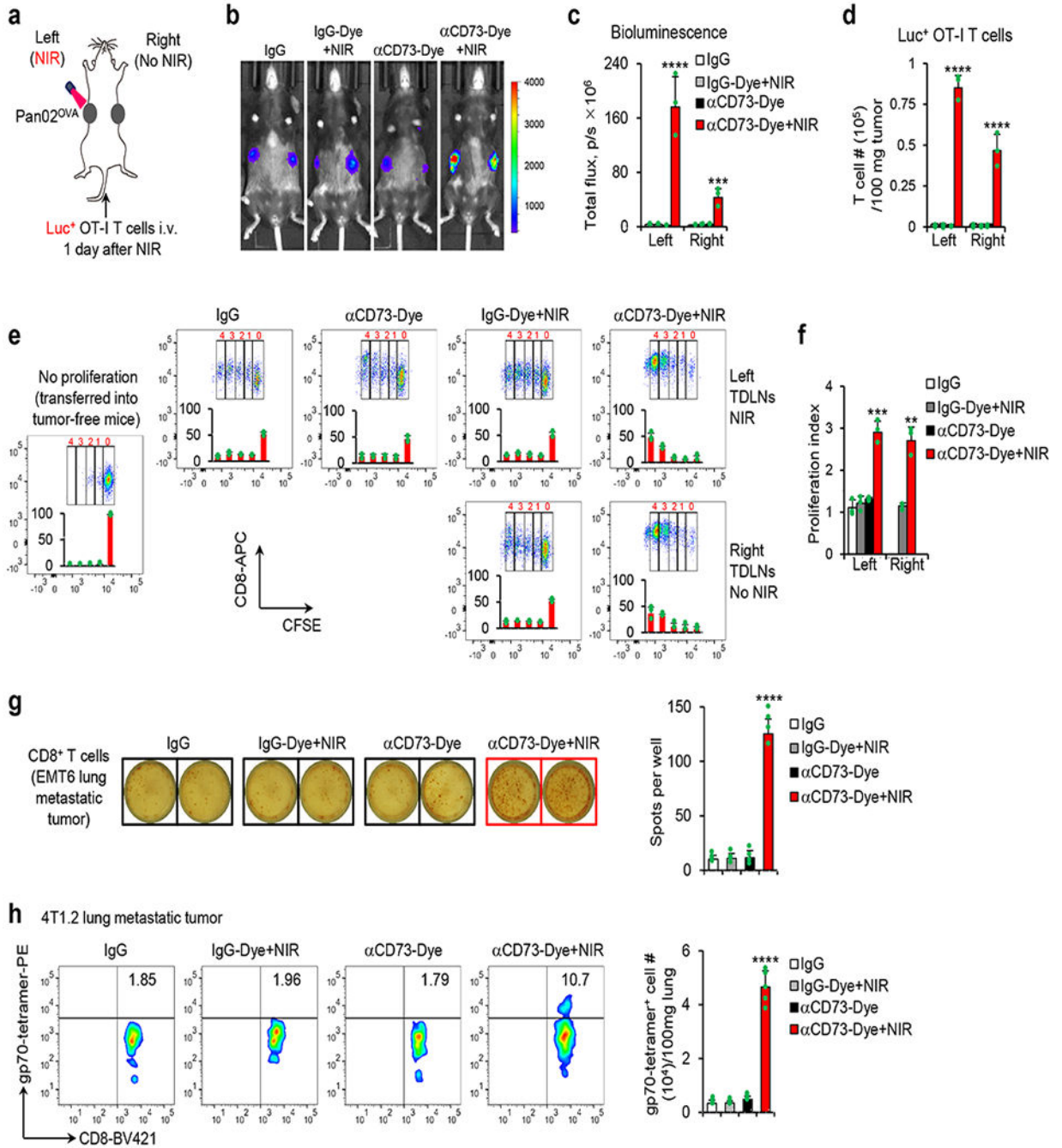


Fig. 4 | Local αCD73-Dye+NIR irradiation favors systemic CTL responses.

(a) Diagram of the treatments. Pan02^{OVA} tumor cells were s.c. injected on the left and right flanks of CD45.1 B6 mice, and treated with IgG, IgG-Dye+NIR, αCD73-Dye, or αCD73-Dye+NIR. NIR performed on the Left-side tumors only (Right-side tumors were shielded from light). One day after NIR irradiation, luciferase-transduced OVA-reactive OT-I T cells were adoptively-transferred via tail vein. Mice were tested for the OT-I T cell accumulation in the tumor. (b) Accumulation of transferred OVA-reactive luciferase-expressing OT-I T cells was tested by *in vivo* Bioluminescence Imaging. Representative images are shown. (c)

Quantitative analysis of transferred OVA-reactive luciferase-expressing OT-I T cells in both left NIR-treated and right non-NIR treated tumors (n=3 biological replicates). **(d)** Calculated cell numbers per 100 mg tumor are shown (n=5 biological replicates/ α CD73-Dye+NIR group, n=4 biological replicates/other groups). The number of CD45.2⁺CD8⁺ OT-I T cells is determined by FACS. **(e)** Pan02^{OVA} tumor cells were s.c. injected on the left and right flanks of CD45.1 B6 mice, and treated with IgG, IgG-Dye+NIR, α CD73-Dye, or α CD73-Dye+NIR. NIR performed on the Left-side tumors only (Right-side tumors were shielded from light). One day after NIR irradiation, CFSE-labeled OT-I T cells were adoptively transferred via tail vein. Mice were tested for cell proliferation in tumor-draining lymph nodes (TDLNs). The proliferation of CFSE-labelled naïve OT-I CD8⁺ T cells in TDLNs of left NIR-treated and right non-NIR treated tumors. Representative data are shown (n=3 biological replicates). **(f)** The proliferation index of CFSE-labelled naïve OT-I CD8⁺ T cells in TDLNs of left NIR-treated and right non-NIR treated tumors are shown (n=3 biological replicates). **(g)** BALB/c mice were inoculated at the left mammary gland with 5×10^5 EMT6 tumor cells and i.v. injection with 1×10^5 EMT6 tumor cells (which allows lung tumor metastasis). IgG, IgG-Dye+NIR, α CD73-Dye, or α CD73-Dye+NIR treatments were given on day 5 to orthotopic tumors when the tumor size reached around 130 mm^3 (other parts of mice were shielded from light). ELISpot analysis measuring IFN γ ⁺ spots derived from CD8⁺ T cells isolated from ~100 mg lung metastatic tumor tissues 10 days after the mice treated as indicated. Representative data and summarized results are shown (n=4 biological replicates). **(h)** BALB/c mice were inoculated at the left mammary gland with 5×10^5 4T1.2 tumor cells and i.v. injection with 1×10^5 4T1.2 tumor cells (which allows lung tumor metastasis). IgG, IgG-Dye+NIR, α CD73-Dye, or α CD73-Dye+NIR treatments were given on day 7 to orthotopic tumors when the tumor size reached around 130 mm^3 (other parts of mice were shielded from light). FACS analysis of gp70 tetramer-positive CD8⁺ T cells in the lung metastatic tumor tissues (n=5 biological replicates) 10 days after NIR. Representative results from one of two repeated experiments are shown. Data are mean \pm SD. ** $P=0.0012926$, α CD73-Dye+NIR group compared with α CD73-Dye group; *** $P<0.001$, **** $P<0.0001$, α CD73-Dye+NIR group compared with IgG, IgG-Dye+NIR, or α CD73-Dye group (**c**, **d**, **f**, **g**, and **h**), one-way ANOVA with Tukey's correction.

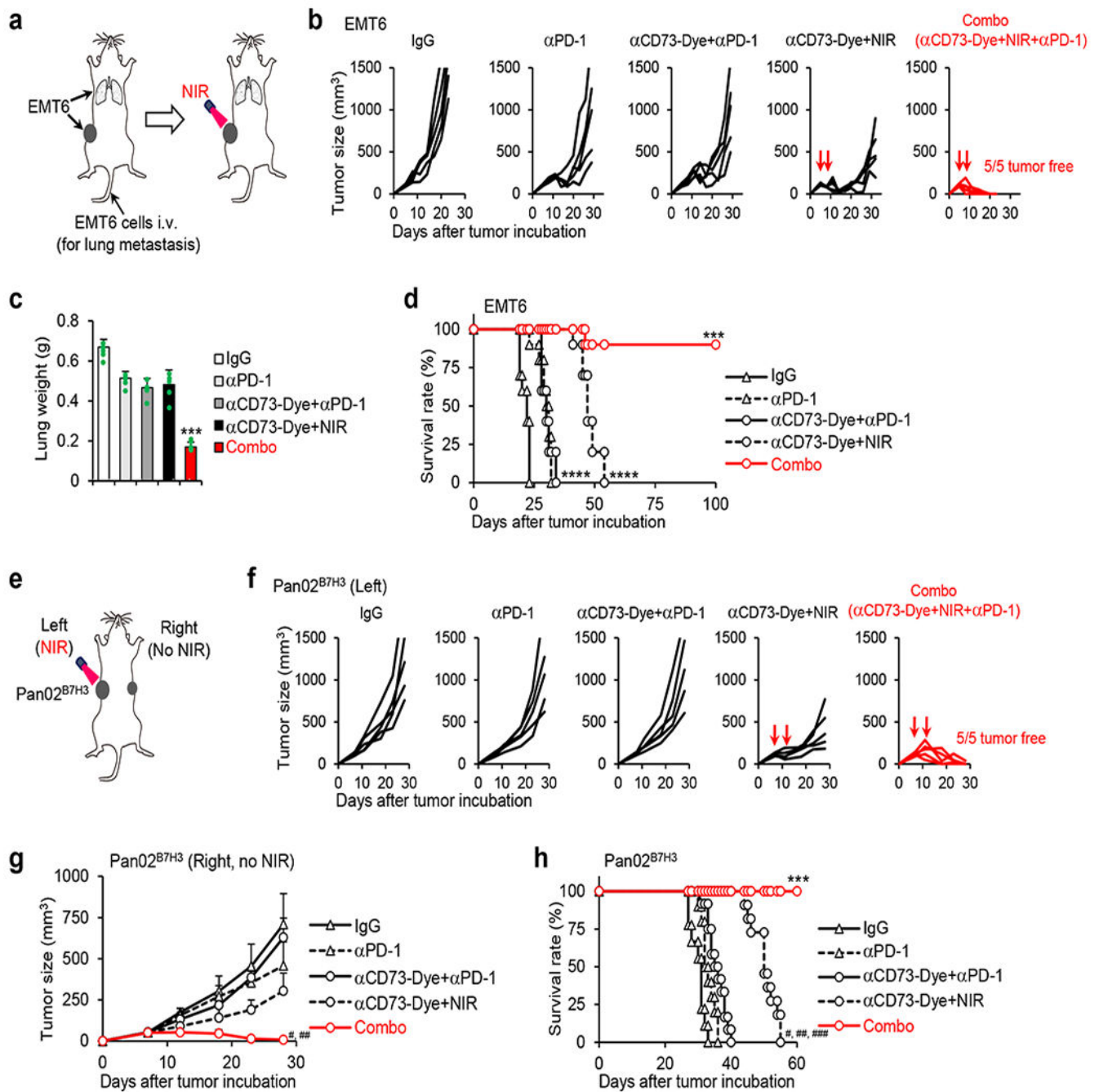


Fig. 5 | α CD73-Dye+NIR irradiation synergizes with α PD-1 ICB to promote curative responses.

(a) Diagram of the treatments. BALB/c mice bearing both orthotopic EMT6 tumor (5×10^5 EMT6 tumor cells injection in the mammary gland) and lung metastasis tumors (1×10^5 EMT6 tumor cells injection via tail vein) were treated on day 5 with control IgG, α PD-1, α CD73-Dye+ α PD-1, α CD73-Dye+NIR, or α CD73-Dye+NIR+ α PD-1 (Combo). NIR irradiation was given on the orthotopic tumor only (other parts of the mice were shielded from light). (b) Tumor growth curves (n=5 mice/group) of the orthotopic EMT6 tumors after indicated treatments. (c) Mice were euthanized on day 20 and the summarized lung weight

of mice receiving indicated treatments are shown (n=5 mice/group). **(d)** Surviving curves of EMT6 tumor-bearing mice (n=10 mice/group). **(e)** Diagram of the treatments. Pan02^{B7H3} tumor cells were s.c. injected on the left (2×10^6 Pan02^{B7H3} cells) and right (5×10^5 Pan02^{B7H3} cells) flanks of B6 mice, and treated on day 7 with control IgG, α PD-1, α CD73-Dye+ α PD-1, α CD73-Dye+NIR, or α CD73-Dye+NIR+ α PD-1 (Combo). NIR performed on the left-side tumor only (right-side tumors were shielded from light). **(f)** Tumor growth curves of NIR-treated left tumors are shown (n=5 mice/group). **(g)** Tumor growth curves of non-NIR-treated right tumors are shown (n=5 mice/group). **(h)** Surviving curves of Pan02^{B7H3} tumor-bearing mice are shown (n=9 mice/IgG group, n=10 mice/ α PD-1 group, n=12 mice/ α CD73-Dye+ α PD-1 group, n=11 mice/other groups). Representative results from one of two repeated experiments are shown. Data are mean \pm SD. *** $P < 0.001$, Combo group compared with IgG, α PD-1, α CD73-Dye+ α PD-1, or α CD73-Dye+NIR group, one-way ANOVA with Tukey's correction **(c)**. *** $P < 0.001$, Combo group compared with IgG, α PD-1, α CD73-Dye+ α PD-1, or α CD73-Dye+NIR group; **** $P < 0.0001$, α PD-1 group compared with IgG group; **** $P < 0.0001$, α CD73-Dye+NIR group compared with IgG, α PD-1, or α CD73-Dye+ α PD-1 group, survival analysis was conducted by log-rank test with holm test for multiple comparisons **(d)**. # means ** $P = 0.00747$, Combo group compared with α CD73-Dye+NIR group, ## means *** $P < 0.001$, Combo group compared with IgG, α PD-1, or α CD73-Dye+ α PD-1 group, two-way ANOVA with Holm-Sidak test for multiple comparisons **(g)**. # means * $P = 0.02969$, α CD73-Dye+NIR group compared with IgG group; ## means ** $P = 0.00983$, α CD73-Dye+NIR group compared with α PD-1 group; ### means * $P = 0.01052$, α CD73-Dye+NIR group compared with α CD73-Dye+ α PD-1 group; *** $P < 0.001$, Combo group compared with IgG, α PD-1, α CD73-Dye+ α PD-1, or α CD73-Dye+NIR group, survival analysis was conducted by log-rank test with holm test for multiple comparisons **(h)**.

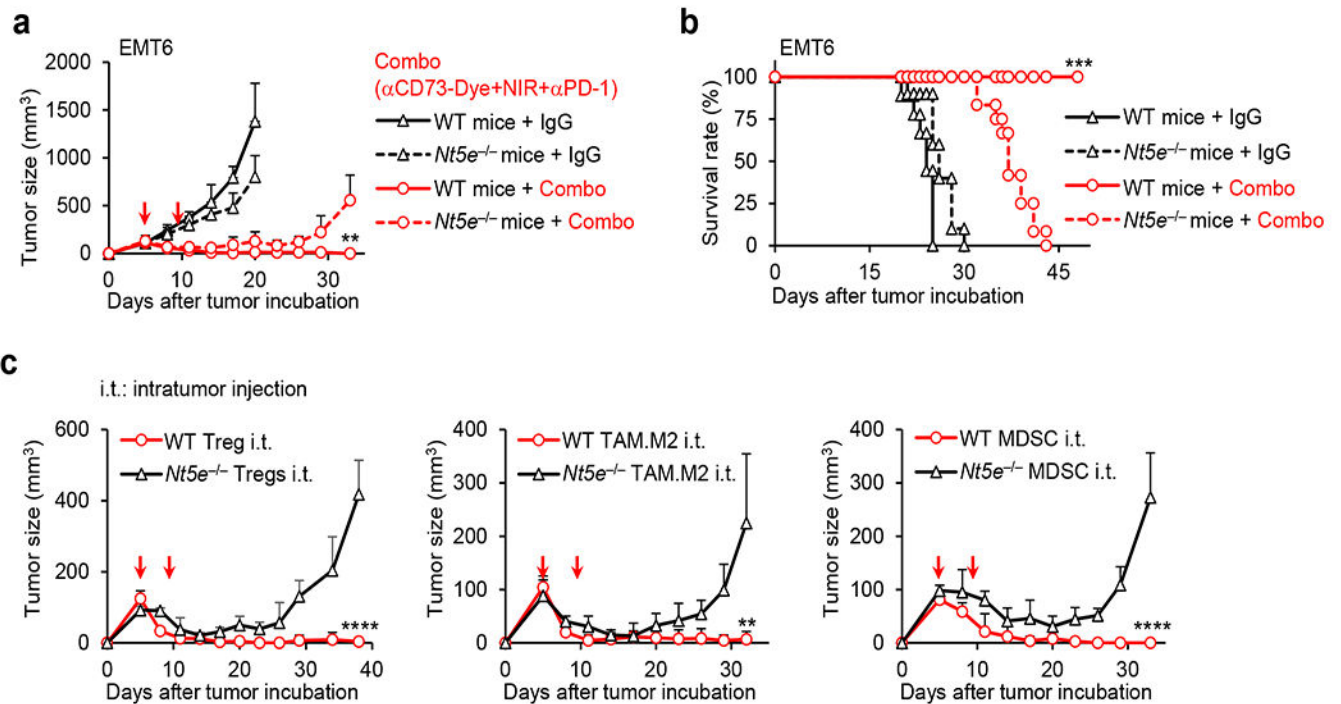


Fig. 6 | Targeting all major types of immunosuppressive cells in tumors is indispensable to the curative response.

Tumor growth curves (**a**, $n=5$ mice /group) and mice survival (**b**, $n=9$ mice/WT mice+IgG group, $n=12$ mice/*Nt5e*^{-/-} mice+Combo group, $n=10$ mice/other groups) are shown after wild-type (WT) or *Nt5e*^{-/-} BALB/c mice bearing 5-day orthotopic EMT6 tumors treated with control IgG or αCD73-Dye+NIR+αPD-1 (Combo). (**c**) Tumor growth curves of reconstituted EMT6 tumors after αCD73-Dye+NIR+αPD-1 combo therapy. Sorted Tregs (Left), TAM.M2 (Middle), or MDSCs (Right) from tumors of EMT6-bearing wild-type (WT) BALB/c mice or *Nt5e*^{-/-} BALB/c mice were intratumorally injected into EMT6 tumors of WT BALB/c mice 1 day before αCD73-Dye+NIR+αPD-1 combo therapy ($n=5$ mice/group). Representative results from one of two repeated experiments are shown. Data are mean ± SD. ** $P=0.00268$, WT mice+Combo group compared with *Nt5e*^{-/-} mice+Combo group, two-way ANOVA with Holm–Sidak test for multiple comparisons (**a**). *** $P<0.001$, WT mice+Combo compared with WT mice+IgG, *Nt5e*^{-/-} mice+IgG, or *Nt5e*^{-/-} mice+Combo, survival analysis was conducted by log-rank test with holm test for multiple comparisons (**b**). ** $P=0.00569$, WT TAM.M2 i.t. group compared with *Nt5e*^{-/-} TAM.M2 i.t. group; **** $P<0.0001$, WT Treg i.t. group compared with *Nt5e*^{-/-} Treg i.t. group, WT MDSC i.t. group compared with *Nt5e*^{-/-} MDSC i.t. group, two-way ANOVA with Holm–Sidak test for multiple comparisons (**c**).

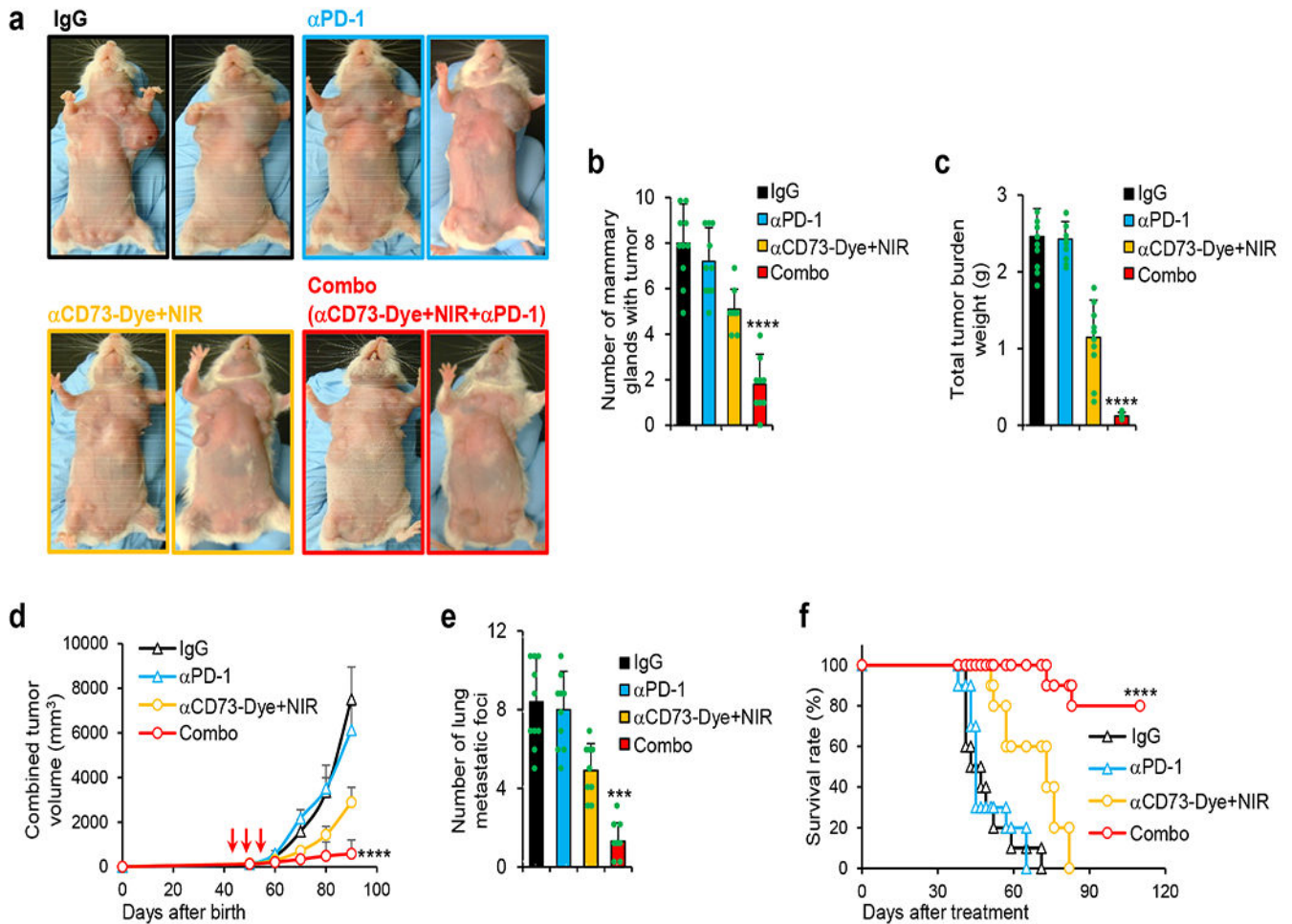


Fig. 7 | α CD73-Dye+NIR irradiation synergizes with α PD-1 to eradicate spontaneous TNBCs. (a) The treatments were initiated when MMTV-PyVT transgenic female mice developed 2 to 3 tumors and each of them reached $\sim 60\text{mm}^3$ (around 6-7 weeks of age), and NIR irradiation was performed on all of these tumors (three α CD73-Dye+NIR treatments in total at weekly intervals; five α PD-1 injections at 3-day intervals). Shown are representative pictures of MMTV-PyVT transgenic female mice treated by IgG, α PD-1, α CD73-Dye+NIR, or α CD73-Dye+NIR+ α PD-1 combo therapy on day 90 after birth. The number of tumor-bearing mammary fat pads (b), total tumor weight (c), combined tumor volume (d), the number of lung metastatic foci (e), and the survival curves (f) of MMTV-PyVT transgenic female mice treated by IgG, α PD-1, α CD73-Dye+NIR, or α CD73-Dye+NIR+ α PD-1 combo therapy ($n=10$ mice/group). Representative results from one of two repeated experiments are shown. Data are mean \pm SD. *** $P<0.001$, **** $P<0.0001$, Combo group compared with IgG, α PD-1, or α CD73-Dye+NIR group, one-way ANOVA with Tukey's correction (b, c, and e); **** $P<0.0001$, Combo group compared with IgG, α PD-1, or α CD73-Dye+NIR group, two-way ANOVA with Holm-Sidak test for multiple comparisons (d). **** $P<0.0001$, Combo group compared with IgG, α PD-1, or α CD73-Dye+NIR, survival analysis was conducted by log-rank test with holm test for multiple comparisons (f).